UNIVERSITY OF CALIFORNIA SAN DIEGO

Maximizing information transmission under threshold modulation via inhibitory neurons

A dissertation submitted in partial satisfaction of the
requirements for the degree
Doctor of Philosophy

in

Physics

by

Wei-Mien Hsu

Committee in charge:

Professor Tatyana O. Sharpee, Chair
Professor David Kleinfeld, Co-Chair
Professor Elena F. Koslover
Professor Terrence J. Sejnowski
Professor Charles F. Stevens

2021

The dissertation of Wei-Mien Hsu is approved, and it is acceptable in quality and form for publication on microfilm and electronically:

_____

_____

_____

_____
Co-Chair

_____
Chair

University of California San Diego

2021

DEDICATION

To those who have supported me throughout *le voyage*.

EPIGRAPH

We know the past but cannot control it.

We control the future but cannot know it.

— Claude Shannon

TABLE OF CONTENTS

Signature Page iii

Dedication iv

Epigraph v

Table of Contents vi

List of Figures viii

List of Tables ix

Acknowledgements x

Vita xi

Abstract of the Dissertation xii

Chapter 1 Introduction 1

Chapter 2 Maximally informative encoding strategies of a single neuron under the metabolic constraints 4
2.1 Neural encoding model and mutual information 5
2.2 Information transmission of a single neuron 8
2.3 Maximally informative encoding with energy constraint 10
2.4 Test of information maximization subject to the energy-constrained 13

Chapter 3 Maximally informative encoding strategies for groups of neurons 16
3.1 Neural responses and mutual information 17
3.2 Maximally informative encoding thresholds for a pair of neurons . . 20
3.2.1 Optimal neuronal thresholds as a function of mean noise level 20
3.2.2 Test of maximally informative model in retina 23

Chapter 4 The influence of threshold modulation on maximally informative encoding strategies 25
4.1 Maximally informative model in the prescience of threshold modulation 26
4.2 Impact of threshold modulation on information transmission 29
4.3 Test of maximally informative prediction in the presence of threshold modulation 36
4.3.1 Retinal input-output functions are maximally informative under threshold modulation 36

4.3.2 Amacrine cells as a source of threshold modulation for adapting cells . . . 38
4.4 Conclusion . . . 41

Appendix A Data acquisition . . . 44
A.1 Experimental preparation . . . 44
A.2 Intracellular recording . . . 44
A.3 Analysis of inhibition from amacrine cells versus RFs distance . . . 45

Appendix B Impact of threshold modulation on maximally informative threshold positions 47

Appendix C The effect of correlated noise on the optimal threshold separation . . . 50

Appendix D Least-squared-fitting for parameters of the threshold modulation model from the retinal data . . . 52

Bibliography . . . 57

LIST OF FIGURES

Figure 2.1: Encoding model for neural responses. 7
Figure 2.2: Information transmission and the averaged spiking probability of a single neuron. 9
Figure 2.3: Information optimization for single cell. 11
Figure 2.4: Response properties and information transmission as a function of constrained energy. 12
Figure 2.5: Sensitizing cells maximize their capacity under the trade-off between noise reduction and firing rate. 15

Figure 3.1: Maximally informative solutions for a groups of neurons 21
Figure 3.2: Information predicts the optimal thresholds for a pair of neurons given the values of noise level. 22

Figure 4.1: Two-pathway model of information transmission in the presence of threshold modulation. 27
Figure 4.2: Impact of threshold modulation on information transmission. 30
Figure 4.3: Modulation directed to sparsely responding neurons protects against information loss in the presence of modulation 32
Figure 4.4: The maximally informative spike rates among neurons were similar for models with and without threshold modulation. 33
Figure 4.5: Optimal ways to apply modulation for neurons with identical spike rates depend on their rates. 34
Figure 4.6: Modulation induced transition in information transmitted as a function of spike rate. 35
Figure 4.7: Experimentally observed threshold variation matches maximally informative values. 38
Figure 4.8: Maximally informative model with modulation accounts for threshold differences between adapting and sensitizing cells. 39
Figure 4.9: Distance dependent inputs from amacrine to adapting cells. 41

Figure B.1: Long-term information surface. 49

Figure C.1: The effect of correlated noise on the optimal threshold separation between the neural types. 51

LIST OF TABLES

Table D.1: Estimated noise components in the primary ν and modulatory σ_μ pathways for each cell pair. 56

ACKNOWLEDGEMENTS

I would like to especially thank my adviser, Prof. Tatyana Sharpee, for her guidance, advice, and supports throughout my Ph.D. study.

I am grateful for the many helpful and inspiring conversations I had with the current and the past CNL-T members. Plus, thanks to Dr. John Berkowitz, Dr. Yilun Zhang, Dr. Ryan Rowekamp, Dr. Joel Kaardal, Dr. Alexander Kuczala, Yuansheng Zhou, Huanqiu Zhang, Dr. Yonatan Aljadeff for essential and enjoyable discussions or supports related to my projects.

I would also like to thank Prof. David Kleinfeld for many interesting conversations and opportunities to teach; Prof. Charles Stevens for insightful discussions and for sharing his stories; my current and past committee members, Prof. Terrence Sejnowski, Prof. Elena Koslover, Prof. Massimo Vergassola, for giving me opportunities to present my work.

I would like to acknowledge our co-author, Dr. David Kastner, and Prof. Stephen Baccus, for sharing their experimental data and valuable comments to our manuscript; Jorge Aldana at Salk CNL for several computational and information technology supports.

Lastly, I would like to thank my parents, Yu-Pong and Yu-Hui, and my sister, Wendy, for supporting whatever I am aiming for; my partner, Maz, for being by my side; my friends for caring and lighting up my life.

Chapter 3, in part, and Chapter 4 in full have been submitted for peer review of the material as it may appear in Cell Reports, Hsu, Wei-Mien; Kastner, David B.; Baccus, Stephen A.; Sharpee, Tatyana O., Cell Press. The dissertation author was the primary investigator and author of this paper.

VITA

2009	B. S. in Physics, National Taiwan Normal University, Taiwan
2011	M. S. in Physics, National Tsing Hua University, Taiwan
2011-2012	Research Assistant, National Taiwan Normal University, Taiwan
2021	Ph. D. in Physics, University of California San Diego

PUBLICATIONS

Hsu, W. M.; Chen, Y. H.; Wang, J. S.; Ite, A. Y. "Slow and stored light pulses in the presence of magnetic fields", *JOSA B* 30, 8 (2013), 2123-2129.

Hsu, W. M.; Kastner, D. B.; Baccus, S. A.; Sharpee, T. O. "How inhibitory neurons increase information transmission under threshold modulation", *bioRxiv*, doi: 10.1101/2020.12.13.422611 (2020).

ABSTRACT OF THE DISSERTATION

Maximizing information transmission
under threshold modulation via inhibitory neurons

by

Wei-Mien Hsu

Doctor of Philosophy in Physics

University of California San Diego, 2021

Professor Tatyana O. Sharpee, Chair
Professor David Kleinfeld, Co-Chair

Information maximization has been one of the guiding principles for understanding sensory neural processing. Given the framework, our goal is to explain nonlinear processing by a group of neurons in the retina, encoding the same filter inputs. We begin with a single-cell model, then extend to a neural population subject to relevant constraints, including metabolic costs and neural noise. Still, their predictions only explain part of the observation. Ultimately, we introduce an extra factor, the noise due to modulation, for better elucidating the retina data.

Modulation of neuronal thresholds is ubiquitous in the brain. Phenomena such as figure-

ground segmentation, motion detection, stimulus anticipation, and shifts in attention all involve changes in a neuron's threshold based on signals from larger scales than its primary inputs. However, this modulation reduces the accuracy with which neurons can represent their primary inputs, creating a mystery as to why threshold modulation is widespread in the brain. We find that modulation is less detrimental than other forms of neuronal variability. Its adverse effects can be nearly eliminated if modulation is applied selectively to sparsely responding neurons in a circuit by inhibitory neurons. We verify these predictions in the retina, where we find that inhibitory amacrine cells selectively deliver modulation signals to sparsely responding ganglion cell types. Our findings elucidate the central role that inhibitory neurons play in maximizing information transmission under modulation.

Chapter 1

Introduction

The need to use efficient representations within the nervous system currently provides one of the leading frameworks for understanding neural computation. Efficiency can be defined in many ways, from maximizing information transmitted about incoming stimuli to minimizing estimation errors. These measures of efficiency are interrelated and often produce similar predictions for neural circuit properties. For example, application of information maximization principles in conjunction with metabolic constraints associated with neural spiking could explain the existence of different types of ganglion cells in the retina tuned to different types of spatiotemporal features [3, 42, 22, 8, 33, 15, 53, 18, 19, 5, 43] and account for many nonlinear aspects of these neural responses [29, 27, 19].

In general, to test the theory of efficient neural computation, one needs to account for several factors/parameters based on the experimental setup and observations. These factors includes metabolic cost, linear/nonlinear tuning properties (e.g. receptive fields, neural input-output relation), input statistics, size of the neuronal population [27, 11, 51], etc. Some of the factors serves as the constraints of the optimization problem, while the others are kept as the ground truths and will be compared with the predictions.

Chapter 2 focuses on the information transmission of a single neuron with the binary

response subject to different constraints. These constraints are generally associated with the neural response properties, such as (1) neural noise, a factor proportional to the tuning width of neural nonlinearity, and (2) spiking probability that affects the metabolic cost. Notably, we propose a constraint that couples the neural noise and spike probability, and demonstrate that its optimal solutions can explain the neural response properties observed in some, but not all, of the retinal ganglion cell types.

Chapter 3 explores the maximally informative strategies for a group of neurons encoding the same scalar inputs. We are particularly interested in the threshold coordination between neurons subject to two factors, the spiking probability, and the neural noise. Note that, unlike the coupled constraint introduced in Chapter 2, we will treat the spiking probability and neural noise as two constraints determined via experimental data. We restraints the degrees of freedom in the optimization for the sake of saving computational time, yet we reserve the rooms for predicting the threshold configuration. The theoretical results for a neuron pair qualitatively explain the emergence of two types of Off retinal ganglion cells (RGCs) encoding the same temporal fluctuations of light intensities but with different thresholds [25]. However, when it comes to the quantitative comparison, the predictions in threshold differences between the neural pairs yielded values that were systematically larger than those observed experimentally [27].

Other theoretical work has pointed out that incorporating multiple noise sources could affect the predictions for threshold differences between cell types [11]. In contrast, our former formalism assumed that the measured neural noise came from the same neural processing stage of the retinal circuit. After testing different scenarios, we found an alternative model with two noise sources: (1) noise from neural nonlinearity in the primary pathway; (2) a secondary pathway modulated the threshold of the primary pathway for each cell type (c.f. Chapter 4, Box 4.1). This model could quantitatively account for the measurements of threshold differences between cell types, across several different contrasts.

In Chapter 4, much attention has been given to investigating how the additional noise

source–the modulatory effects on cells' thresholds–in conjunction with the noise in the primary pathway, affects information transmission. For a sensory circuit, modulation of neuronal threshold independent of the primary sensory input is bound to decrease the information that this circuit can transmit about that primary input. Nevertheless, modulation always decreases information less than an equivalent increment in primary noise. Furthermore, modulation's negative impact is nearly ignorable if directed to a subset of sparsely responding neurons in a coupled neural circuit. Indeed, after fitting the maximally informative model with threshold modulation to the retinal data, we found that one of the cell types with high threshold experiences more extensive threshold modulations than the other with low threshold. On the other hand, the primary pathway noise levels were similar for both cell types. These also explained why higher noise levels, a nonlinear sum of the two types of noise, were observed in high-threshold cells compared to low-threshold ones. Regarding the causes of threshold modulation, our analysis from a separate experiment indicated that amacrine cells send stronger inhibitory inputs to the high-threshold cell than to the low-threshold one. It is consistent with the scheme where high-threshold neurons get more inhibitory input for regulating the activity and, therefore, respond sparsely and have more noise.

Overall, this dissertation focuses on explaining nonlinear processing for a group of neurons in the retina, assuming that sensory circuitry optimizes their neural code to encode sensory information efficiently. We started with a single-cell model, then extended to a neural population subject to relevant constraints. Finally, we consider an additional noise caused by threshold modulation, for better clarifying the retina data. All theoretical results shown here are based on the basic concepts of information theory. Therefore, they should apply not only in the retina but also in other neural circuits.

Chapter 2

Maximally informative encoding strategies of a single neuron under the metabolic constraints

Efficient coding posits that, given internal constraints (e.g., metabolic resources), sensory systems optimize their neural code for transmitting maximal information about sensory inputs. Mutual information maximization framework has been one of the guiding principles for understanding neural computation, and it accounts for a number of different properties of neural responses [7, 3, 42, 22, 8, 33, 15, 53, 18, 19, 5, 43, 29, 27, 11], including optimal ways for neural circuits to adapt to statistically consistent changes in the input statistics [7, 16, 47, 9].

To test maximally informative solutions on experimental observation, one needs to consider one or a set of internal constraints, including metabolic cost [7, 31, 30, 53, 5], linear/nonlinear tuning properties (e.g. receptive fields, neural input-output relation) [29], input statistics, size of the neuronal population [27, 11, 51], etc. This chapter focuses on two factors: metabolic cost, related to neural spiking rate, and the width of neural nonlinearity, which we denote as 'neural noise.' Metabolic cost strongly impacts maximally informative solu-

tions [53, 7]. Generally, the capacity for transmitting information increases with the average spike rate [44] and, for binary responses, reaches its peak at 50% of the maximally achievable rate. Nevertheless, many neurons in the brain respond at much lower rates [40]. This is thought to occur because high response rates incur the disproportionately large metabolic cost [5, 31]. Meanwhile, for any given average spike rate, the information capacity increases as the noise level decreases and reaches its extreme at zero noise value that is not biologically realistic.

Considering a single binary neuron, we predict a family of optimal encoding solutions subject to a newly defined 'energy' constraint that incorporates average spike rate and neural noise. We test the predictions on OFF retinal ganglion cells (RGCs) and find one of the cell types operates over a range of energies, adjusting both the noise level and spike rate to follow the maximally informative solutions. The other cell types follow the contours of constant energy rather than the predicted optimal solutions.

Based on the experimental setup and the measurements, the two types of OFF RGCs encoded the same temporal fluctuations of light intensities but with different thresholds. This threshold coordination between the two cell types suggests that they might work together, and one should consider their joint neural responses for predicting the informative solutions. Thus, the next chapter will focus on the information maximization for a group of neurons jointly encoding the same filtered inputs.

2.1 Neural encoding model and mutual information

This section provides the formalism to quantify the information transmitted by a single-neuron. We consider a neuron as a communication channel that encodes the scalar stimulus x with prior $p(x)$ into its binary activities, either $r = 0$ (silence) or 1 (spike). Firstly, we define the neural response, an mathematical abstraction of input/output relation, as the probability to elicit the response r for a given stimulus x, $p(r|x)$. With the neural responses, one can compute the

average spiking probability and the mutual information between neuronal response and stimulus. This single-neuron model can be extended to a group of N neurons that jointly encode the same filtered stimulus values (c.f. Chapter 3).

Model of neural response

We model responses of a single neuron as binary variable, $r = 1$ or 0, corresponding to the presence or absence of a spike in a small time bin, respectively. Spiking probability is modeled as a threshold crossing event. Here, we use a saturating sigmoid function (normal cumulative distribution function, Fig. 2.1) to describe the probability to elicit a spike ($r = 1$) for a given filtered stimulus (x),

$$p(r=1|x) = p(r=1|x,\mu,\nu) \tag{2.1}$$

$$= \frac{1}{2}\left[1+\mathrm{erf}\left(\frac{x-\mu}{\sqrt{2}\nu}\right)\right], \tag{2.2}$$

and $p(r=0|x) = 1-p(r=1|x)$ is the probability to be silent. Neuronal threshold (μ) sets the stimulus value corresponding to 50 % spiking probability. Neural noise (ν) determines the variation in neural responses for a given input value relative to the threshold ($x-\mu$) : when ν is small, there is only a small range of stimuli for which neuronal responses varies from trial-to-trial, as reflected by spike probabilities ~ 0.5. When parameter ν is large, the range of stimuli with uncertain neuronal responses is greater. For inputs that are either much greater or smaller than the threshold μ, the spike probability is nearly certain, with values close to either 1 or 0, cf. Fig. 2.1. The increase in the uncertainty in neural responses with ν can be quantified using a quantity known as noise entropy [10], which represents the average uncertainty in the neural responses across different stimuli.

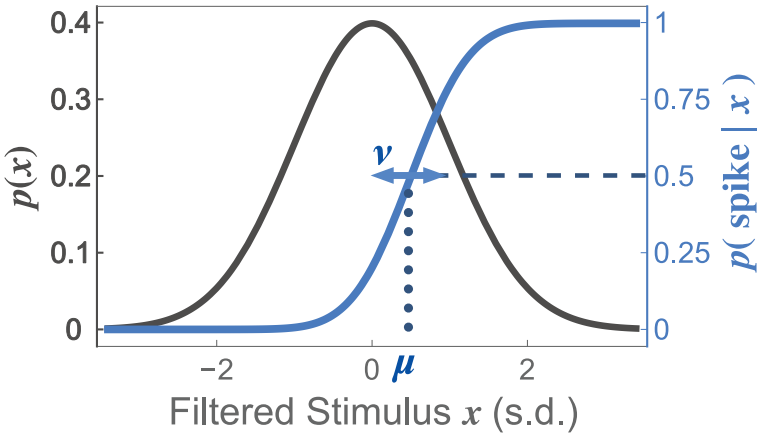

Figure 2.1: **Encoding model for neural responses.** The static nonlinear function of a cell (blue) maps the filtered stimulus x onto a spiking probability ranging between zero and one. The x-axis is scaled by the standard deviation of filtered stimulus (gray).

Averaged neural responses

Averaging the neural response $p(r|x)$ across all possible stimulus $x \in X$ gives the total probability to spike ($r = 1$) or of being silence ($r = 0$),

$$p(r) = \int_{-\infty}^{\infty} dx\, p(r|x)\, p(x)\,, \tag{2.3}$$

where $p(x)$ is the probability density function of filtered stimulus. If $p(x)$ is a Gaussian distribution with mean x_0 and standard deviation σ_x, we get nice form for the average responses,

$$p(r=1) = \frac{1}{2}\left[1 - \mathrm{erf}\left(\frac{\mu - x_0}{\sqrt{\nu^2 + \sigma_x^2}\sqrt{2}}\right)\right], \tag{2.4}$$
$$p(r=0) = 1 - p(r=1)\,.$$

Mutual Information

To quantify the average amount of information the neural responses ($r \in R$) conveys about the filtered stimulus ($x \in X$), we compute the mutual information between the two variables, R and X [13],

$$I(X;R) = \int dx \sum_{r\in R} p(r,x) \log_2 \frac{p(r,x)}{p(r)\,p(x)}, \tag{2.5}$$

$$= \int dx\, p(x) \sum_{r\in R} p(r|x) \log_2 \frac{p(r|x)}{p(r)}, \tag{2.6}$$

where $p(r|x)$ is the neural responses given by Eq. 2.2 and $p(x)$ is the probability density function of the filtered stimulus (x).

In next section, we revisit the results of how the information changes with the spike rate and neuronal noise, and show the optimal encoding strategies under this model framework.

2.2 Information transmission of a single neuron

We will review how the neural noise and the average spike probability affects information transmission regarding the single-neuron case. Given the neural response function (Eq. 2.2) and that the stimulus $p(x)$ is a Gaussian distribution with mean x_0 and standard deviation σ_x, we can compute the mutual information between the stimulus and the neural responses, $I(X;R)$ (Eq. 2.6) (Fig. 2.2 (A)). The same applies to the average spike probability, p_{spike} (Eq. 2.4) (Fig. 2.2 (B)). Note that both $I(X;R)$ and p_{spike} shown in Fig. 2.2 are straightforwardly represented in the space of the neural threshold (μ) and noise level (ν), which are parameters of the response function (Eq. 2.2). To better illustrate how the information depends on neural noise and average spike probability, we remap the parameters of information from the space of (μ,ν) onto that of $\left(p_{\text{spike}},\nu\right)$ (Fig. 2.3 (A)) based on Fig. 2.2 (A)(B).

Figure 2.3 (A) to (C) summarize two main observations: (1) the average spike probability (p_{spike}) considered by itself increases information until p_{spike} reaches the half of its maximal value (Fig. 2.3 (B)); (2) similarly, the noise (ν) when considered separately from other parameters decreases information transmission (Fig. 2.3 (C)). Both of these effects are well established in

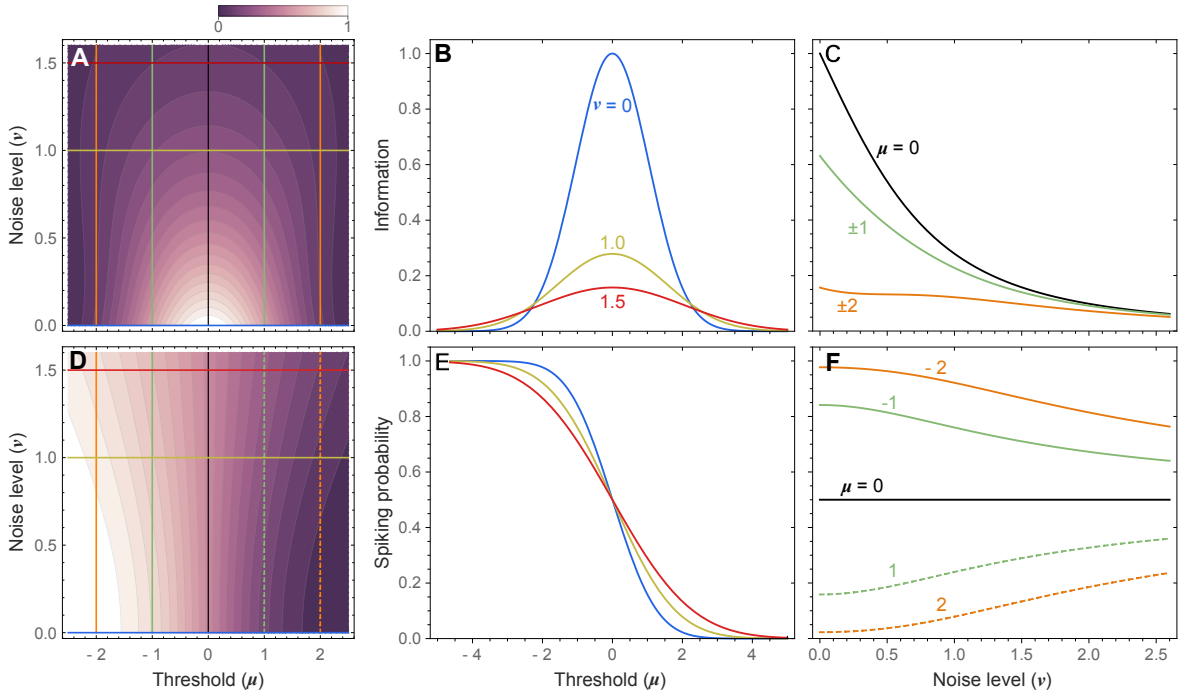

Figure 2.2: **Information transmission and the averaged spiking probability of a single neuron.** (**A**) Information contours as a function of threshold (μ) and neural noise level (ν). Here, the threshold (ν) is relative to the mean of the filtered input (Fig. 2.1) and both ν and μ are in the unit of stimulus standard deviation, σ_x. (**B**) Information always peaks at $\mu = 0$ where spiking probability (p_{spike}) is 0.5 for any constant noise levels (ν). (**C**) The global maximum of information is at $\nu = 0$ for a given threshold (μ). (**D**) The spiking probability contours with the same axes as (A). (**E**) Spiking probability is asymptotic to one (zero) as the threshold (μ) moves further below (above) the input mean. (**F**) Spiking probability increases (decreases) with neural noise (ν) when the threshold (μ) is below (above) the mean of the input, and stays as constant 0.5 as the threshold equals to the input mean ($\mu = x_0 = 0$).

the literature [10, 31]. However, in the biological system, neurons not only fire sparsely over time ($p_{\text{spike}} \ll 50\%$), but also are unlikely to be noiseless ($\nu = 0$), i.e., experimental observed neural response is never going to be a binary step function. One possible reason is that both p_{spike} and ν relate to the metabolic cost. In the next section, we introduce a conceptual model of how the interaction between these two factors can lead to unexpected results.

2.3 Maximally informative encoding with energy constraint

Neurons do not transmit information for no energy consumption. In Sec. 2.2, we reviewed that information transmitted via a neuron depends both on the spiking probability (p_{spike}) and neural noise (ν). Intuitively, both of these factors should relate to some energy (metabolic) quantities. Thus, we formalize total energy consumed per unit time as follows,

$$\varepsilon_{\text{cost}} = p_{\text{spike}} + \Gamma(\nu), \tag{2.7}$$

where p_{spike} is the spiking probability of a neuron, and $\Gamma(\nu)$ is the energy cost dependent on the neural noise. As reducing the neural noise increases information transmission, the function $\Gamma(\nu)$, at the first approximation, can be assumed to be a negative power function of noise level (ν),

$$\Gamma(\nu) = q\nu^{\alpha}, \text{ with } \alpha < 0 \tag{2.8}$$

where the parameter q weights the costs relative to that of spiking,

$$\varepsilon_{\text{cost}}\left(p_{\text{spike}}, q, \nu\right) = p_{\text{spike}} + q\nu^{\alpha}. \tag{2.9}$$

Mutual information between the filtered input (X) and the neuronal responses (R), $I(X;R)$, can be parameterized as a function of spiking probability $p_{\text{spike}}(\mu,\nu) = p(r=1)$ and neural noise ν (Eq. 2.4). The objective is to maximize the information constraining on the available total energy $\varepsilon_{\text{cost}}$

$$\begin{aligned} &\arg\max_{p_{\text{spike}},\nu} I(X;R) \\ &\text{subject to } \varepsilon_{\text{cost}}\left(p_{\text{spike}}, q, \nu\right) \leq \varepsilon_{\max}, \end{aligned} \tag{2.10}$$

which predicts the optimal neural response properties, $\left(p_{\text{spike}}, \nu\right)_{\text{opt}}$, or equivalently, $(\mu,\nu)_{\text{opt}}$.

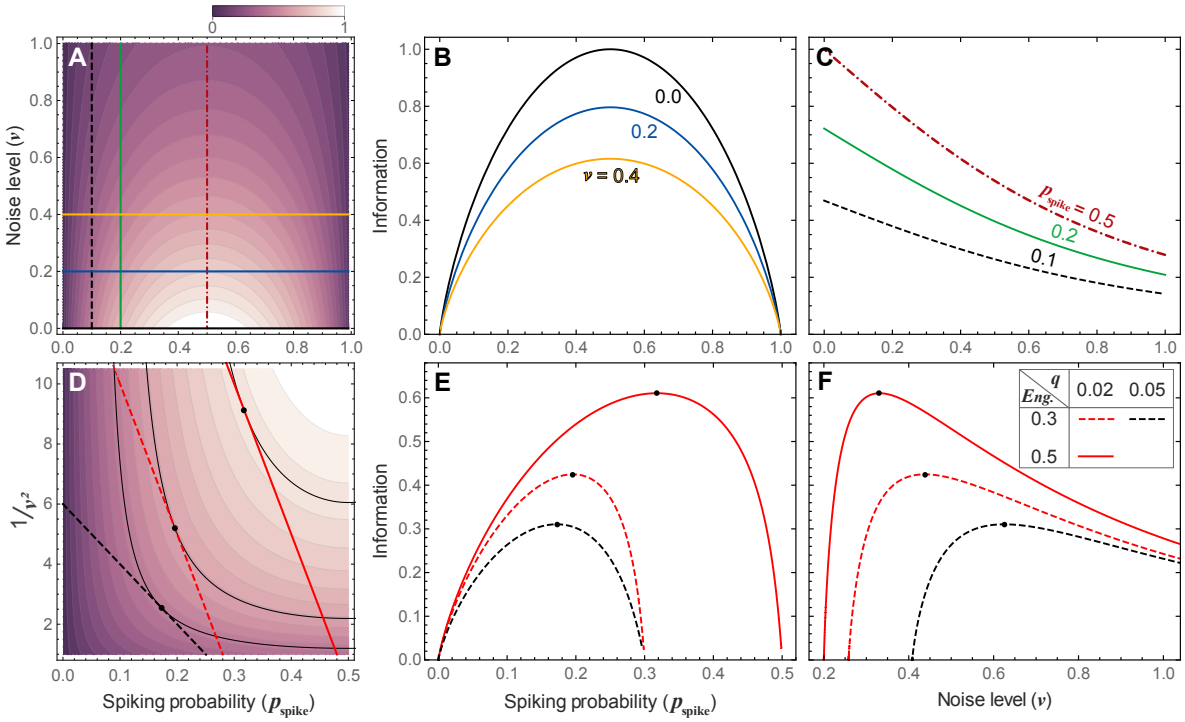

Figure 2.3: **Information optimization for single cell.** (**A**) Information contours as a function of noise level (ν) and spiking probability (p_{spike}). (**B**) Information always peaks at $p_{\text{spike}} = 0.5$ for any constant noise levels (ν). (**C**) Primary noise decreases information for any constant p_{spike}. (**D**) Same as (**A**) but as a function of $1/\nu^2$ and p_{spike}. (**E**) Information peaks at different p_{spike} (black dots) for different energy constraints (Eq. 2.9, with $\alpha = -2$), denoted as three straight lines in (**D**). (**F**) Optimal neural noise changes with different energy constraints.

The predicted solution $(\mu, \nu)_{\text{opt}}$ changes with different sets of $(\varepsilon_{\text{cost}}, q, \alpha)$. Figure 2.3 (D)-(F) shows the examples of fixed $\alpha = -2$ with different $\varepsilon_{\text{cost}}$ and q. At a constant $\varepsilon_{\text{cost}}$, the increase in q makes the cost of noise reduction more expensive and shifts the optimal noise level (ν) to a larger value. Meanwhile, both the optimal spike probability and the attainable information decreases (dashed-lines, Fig. 2.3 (E, F)). At a fixed q, in general, the more the total energy ($\varepsilon_{\text{cost}}$) is, the lower the optimal noise level can be, the closer the spiking rate can reach to 50%, and the higher the information is achieved (red-lines, Fig. 2.3 (E, F)). Figure 2.4 summarizes how the optimal noise level, spiking probability and transmitted information change with the total energy for different sets of (q, α).

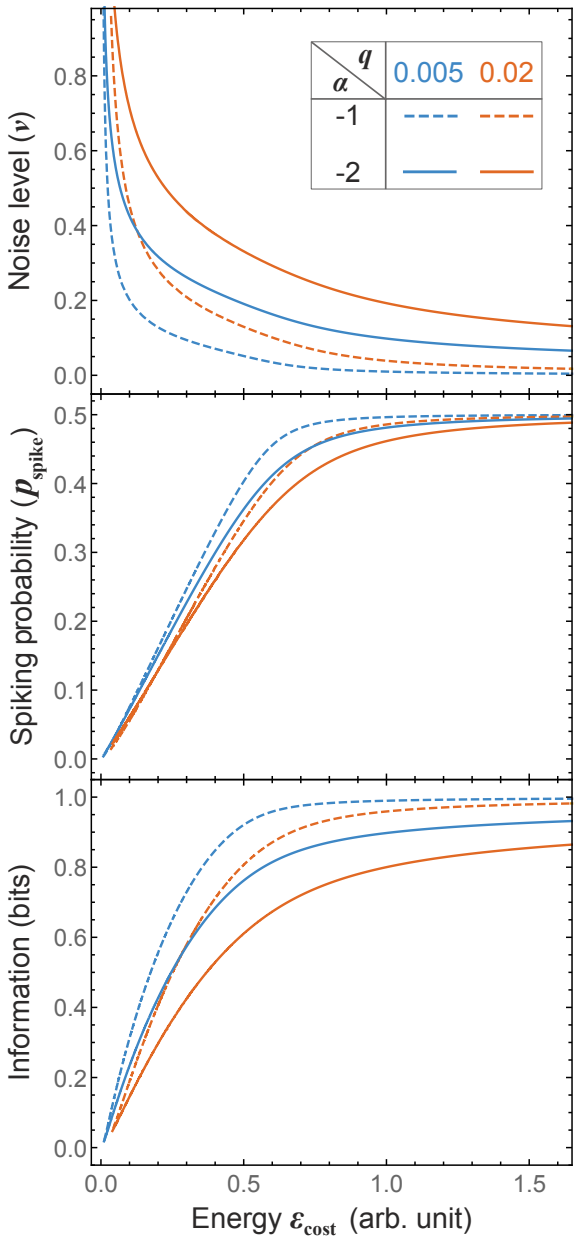

Figure 2.4: **Response properties and information transmission as a function of constrained energy.** (**Top**) Optimal neural noise decreases with the constrained energy. Each line denotes different sets of parameters (q, α) defined in the total energy equation, Eq. 2.9. (**Middle**) Spiking probability (p_{spike}) and (**bottom**) information increases with energy, and asymptotically approaches their best values, 0.5 and 1, respectively. For a given α, smaller q ensures higher p_{spike} and transmits more information.

2.4 Test of information maximization subject to the energy-constrained

We test the predicted maximally informative solutions on the responses of two types of OFF retinal ganglion cells (RGCs) that encode the same temporal fluctuations of light intensities but with different thresholds. These cells have been termed 'adapting' and 'sensitizing' based on their short-term plasticity [25], the main differences between these cell types are that adapting cells have higher thresholds and larger noise levels than sensitizing cells.

We find that some retinal cell types follow contours of constant metabolic cost, e.g. adapting cells in Fig. 2.5. Other cell types, e.g. the sensitizing cells operate over a range of metabolic rates, adjusting both the primary noise and spike rate to follow the maximally informative contours. These analyses stay qualitatively the same for different definitions of metabolic cost. Here, we used a weighted sum of spike rate and inverse primary noise squared,

$$\varepsilon_{\text{cost}} = p_{\text{spike}} + \frac{q}{\nu^2}, \tag{2.11}$$

where parameter q weighs the contributions associated with increasing the firing rate and reducing noise.

We find that all sensitizing cells (except for one outlier cell to be discussed below) balanced noise reduction with firing rate increases across contrasts in a way that aligned with a maximally informative contour with a fixed $q = 0.01 \pm 0.003$ (mean and standard deviation across cells), cf. Fig. 2.5. The outlier sensitizing cell balanced its noise and firing rate in a way that aligned with a constant energy cost, with the same q value as the rest of the sensitizing cells. This sensitizing cell had the highest firing rate, and the fact that its data points aligned with the contour of highest energy across the sample, indicates that it reached its maximal metabolic rate and was forced to deviate from the maximally informative curve that other sensitizing cells

followed. The majority of adapting cells changed their parameters in ways that were similar to the outlier sensitizing cell, except that they limited their overall metabolic cost to a low value. When these cells increase their metabolic energy, they join the same maximally informative curve as the sensitizing cells. Notably, the q parameter for the constant energy contours followed by most adapting cells and the outlier sensitizing cell was the same as that for the maximally informative curve followed by the rest of sensitizing and adapting cells.

Overall, these analyses illustrate that, as a rule, sensitizing cells balance their noise and threshold settings to provide maximal information. These cells can adjust their metabolic parameters over a relatively wide with contrast. In contrast, adapting cells work at low metabolic levels. We will show that the different threshold placements adopted by the two cell types allow for efficient information transmission when considering them together (c.f. Chapter 3). Besides, each cell type impacts information differently when receiving modulatory inputs from a secondary pathway (c.f. Chapter 4).

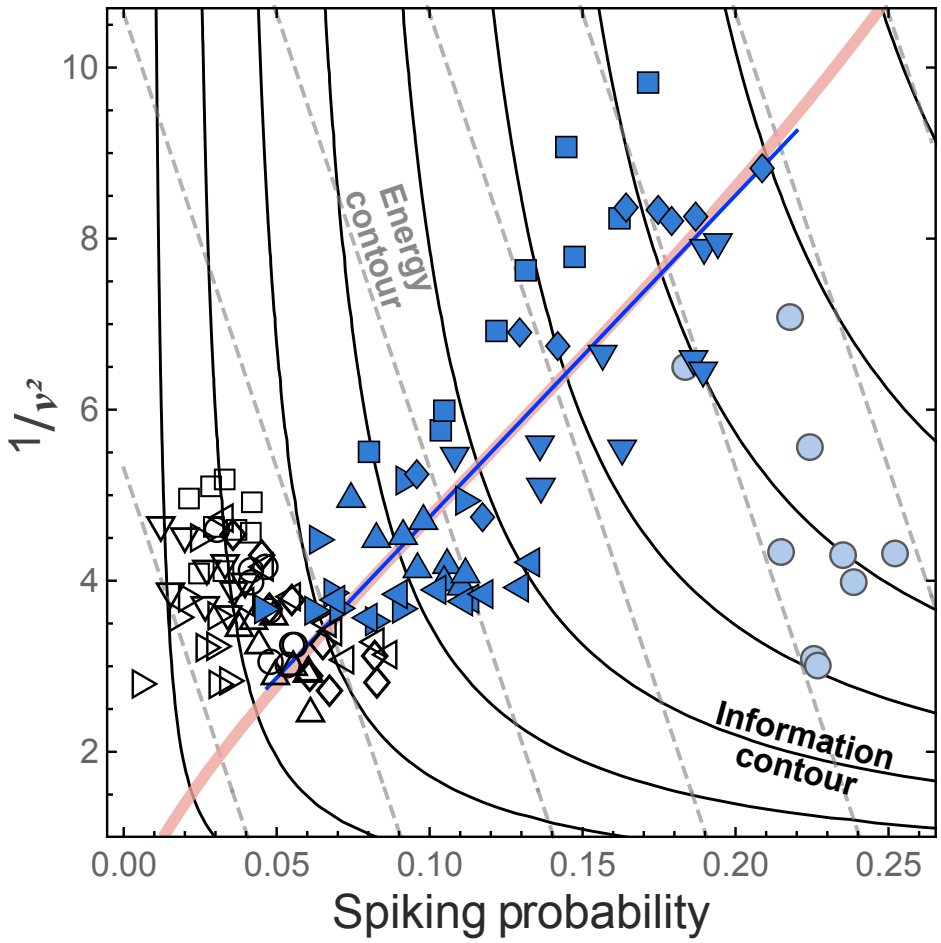

Figure 2.5: **Sensitizing cells maximize their capacity under the trade-off between noise reduction and firing rate.** Adapting (open symbols) and sensitizing (filled) cells adopt different strategies in balancing the metabolic costs of spiking (x-axis) and noise reduction (y-axis). Same symbols (filled or open) denote pairs of sensitizing and adapting cells that were recorded simultaneously, with multiple points representing data for different stimulus contrasts. Most of the sensitizing cells (blue line shows the linear least-squares fitting) follow a maximally informative contours with a fixed q value (pink line). The one outlier sensitizing cell had the highest firing rate (light-blue circles) and aligned with a constant high-energy contour, suggesting that it was energy limited. Most of the adapting cells also followed a constant energy contour (gray dashed lines), but at low value, with a small fraction following the maximally informative contour with the same q value as the sensitizing cells. This supports the notion that adapting cells tend to operate at low constant metabolic costs, increasing their information transmission in a maximal way when necessary.

Chapter 3

Maximally informative encoding strategies for groups of neurons

Sensory systems are designed to maximize the information transmission about the environment through optimizing the neural populations at each level of neural circuitry, across the information pathways. This optimization leads to the emergence of multiple cell types, each of which not only encodes a certain linear (spatial-temporal) feature [29, 3, 9, 42, 22, 8, 33, 15, 53, 18, 19, 27, 5, 43] but also responses with a specific group of nonlinear properties (e.g., thresholds and sensitivity) [36, 38, 25, 19, 27]. For instance, the retinal ganglion cell (RGC) population transmits information more efficiently by having On and Off cell types that maximally respond to different visual features, than doing so with just either one [19]. In addition, recent studies found the Off population, rather than On, responses to the same visual feature with two classes of neural thresholds: Off adapting cells with a higher threshold, and Off sensitizing with a lower one [25].

Here, we review the mutual information framework for a group of neurons encoding the same scalar inputs and show their optimal threshold coordination in conjunction with the constraints. Unlike the constraint stated in Chapter 2, we will take the spiking probability and

neural noise as two ground-truth constraints determined by the experimental data. Although we restraints the degrees of freedom in the information optimization for saving computational resources, we keep the room for predicting the threshold allocations among neurons.

Regarding the hallmark in predictions, as the neural sensory noise lies below a specific value, having a neural population encoding a particular linear feature but with multiple classes of threshold becomes the most optimal encoding strategy [19, 27, 11]. This prediction accounts for the emergence of two types of Off RGCs that have low neural noise, as well as the single type among On cells that have high neural noise.

3.1 Neural responses and mutual information

First, we defined the model of neural response for a group of neurons ($N > 1$) that jointly encode the same stimulus. Our choice of the modeling framework was motivated in part by the experimental setup that used full-field temporally varying stimuli to probe responses of the retinal ganglion cells (RGCs) [25]. Specifically, we were interested in characterizing how two types of fast-Off neurons, the adapting and sensitizing RGCs, jointly encode these temporal fluctuations in light intensity. These two types of neurons have very similar temporal filters [25]. Thus both types of neurons encode the same input component $x(t) = \int (t-\tau)\, s(\tau)\, d\tau$.

Given the neural response that depends on the neural threshold (μ_i) and noise level (ν_i) of each cell, we can compute spiking probability and mutual information as a function of (μ_i, ν_i). Via maximizing information transmission, we calculate the optimal neural thresholds (μ_i) given different neural noises (ν_i) and spiking probabilities.

In the next section, we recap the result that the mean noise level of a cell pair ($N = 2$) controls their optimal thresholds and that it becomes optimal to encode stimulus with different thresholds when the mean noise level is lower than a critical value [36, 27].

Joint response of for a group of neurons

If we consider a group of N binary neurons jointly encoding the same filtered stimulus $(x \in X)$, given the assumption that their responses are "conditionally independent" without significant correlations, the probability of yielding the joint response $\mathbf{r}$ for a given filtered stimulus x is

$$p(\mathbf{r}|x) = \prod_{i=1}^{N} p(r_i|x), \tag{3.1}$$

where the vector $\mathbf{r} = (r_1, r_2, ..., r_N)$ denotes N-neurons' responses with $r_i = \{0, 1\}$, and the response function of individual neuron i, $p(r_i|x) = p(r_i|x, \mu_i, \nu_i)$, is given by Eq. (2.2)

$$p(r_i = 1|x) = \frac{1}{2}\left[1 + \mathrm{erf}\left(\frac{x - \mu_i}{\nu_i\sqrt{2}}\right)\right], \tag{3.2}$$

$$p(r_i = 0|x) = 1 - p(r_i = 1|x). \tag{3.3}$$

Averaged neural responses and total spiking probability

The joint neural response $p(\mathbf{r}|x)$ averaged across the stimulus distribution $p(x)$ gives the averaged probability of response $\mathbf{r}$,

$$p(\mathbf{r}) = \int dx\, p(x)\, p(\mathbf{r}|x), \tag{3.4}$$

$$= \int dx\, p(x) \prod_{i=1}^{N} p(r_i|x). \tag{3.5}$$

where $p(x)$ is the probability density function of filtered stimulus (x). The averaged total spiking probability p_{spike} of N neurons is to sum over the possible 2^N responses $(\mathbf{r} \in \mathbf{R})$ as following

$$p_{\mathrm{spike}} = \sum_{\mathbf{r}\in\mathbf{R}} \|\mathbf{r}\|_1\, p(\mathbf{r}) = \sum_{i=1}^{N} p(r_i = 1), \tag{3.6}$$

$$\|\mathbf{r}\|_1 = \sum_{i=1}^{N} r_i.$$

where $p(r_i = 1)$ is the spiking probability of ith neuron given by Eq. (2.3).

Taking $N = 1$ and 2 as examples, all the possible response $\mathbf{r} \in \mathbf{R}$ and the total spiking probability are summarized as follows:

N	$\mathbf{r}$	$\mathbf{R}$	p_{spike}
1	r_1	$\{1,0\}$	$p(r_1 = 1)$
2	(r_1, r_2)	$\{(1,1),(1,0),(0,1),(0,0)\}$	$p(r_1 = 1) + p(r_2 = 1)$

For $N = 2$, the total spiking probability is the linear sum of individual

$$\begin{aligned} p_{\text{spike}} &= \sum_{\mathbf{r}\in\mathbf{R}} \|\mathbf{r}\|_1 \, p(\mathbf{r}), \\ &= \sum_{\mathbf{r}\in\mathbf{R}} \|(r_1, r_2)\|_1 \, p(\mathbf{r_1}, \mathbf{r_2}) \\ &= 2p(1,1) + p(1,0) + p(0,1), \\ &= [p(1,1) + p(1,0)] + [p(1,1) + p(0,1)], \\ &= p(r_1 = 1) + p(r_2 = 1). \end{aligned}$$

This applies to arbitrary number of N, as given by Eq. (3.6).

Mutual information

Similar to the formalism of single cell (Sec. 2.1), for N neurons $(\mathbf{r} \in \mathbf{R})$ joint encoding the same filtered stimulus, mutual information between their responses $(\mathbf{r} \in \mathbf{R})$ and the stimulus values $(x \in X)$ is given by (cite: 2012 Elements of information theory by Cover, Information Theory by MacKay):

$$I(X;\mathbf{R}) = \int dx \, p(x) \sum_{\mathbf{r}\in\mathbf{R}} p(\mathbf{r}|x) \log_2 \frac{p(\mathbf{r}|x)}{p(\mathbf{r})}, \tag{3.7}$$

where $p(\mathbf{r}|x)$ is given by Eq. (3.1) and $p(x)$ is the probability density function of filtered stimulus.

Given the neural response $p(\mathbf{r}|x)$ that depends on the neural threshold (μ_i) and noise level (ν_i) of each cell, one can compute spiking probability, p_{spike}, and mutual information, $I(X;\mathbf{R})$, as a function of (μ_i, ν_i). Via maximizing information transmission, we calculate the optimal neural thresholds (μ_i) subject to the given constraints: the neural noises (ν_i) and total spiking probabilities (p_{spike}). Figure 3.1 shows the examples of optimal thresholds and individual spiking probability for the two and three neurons cases. In the next section, we recap the result [36, 27] that the mean noise level of a cell pair ($N = 2$) controls their optimal thresholds and that it becomes optimal to encode stimulus with different thresholds when the mean noise level is lower than a critical value.

3.2 Maximally informative encoding thresholds for a pair of neurons

3.2.1 Optimal neuronal thresholds as a function of mean noise level

By considering the case of a neuronal pair ($N = 2$), we recap the theoretical prediction of how the emergence of different neural types is subject to the mean neural noise. For the purpose of our problem, the main differences between these two neuronal types is that they encode the same signal $(x \in X)$ with different thresholds. Thus, our first step is to define the *optimization problem* that predicts the optimal neuronal thresholds, or alternatively, the optimal difference between thresholds of a neuronal pair ($\Delta\mu = \mu_1 - \mu_2$).

For two neurons, both mutual information $I(X;\mathbf{R})$ and spiking probability p_{spike} depends on the four parameters of the encoding model, Eq. (3.1): the thresholds and noise levels of all cells $(\mu_i, \nu_i), \forall i = \{1,2\}$. One can reparametrize the information function from the space of

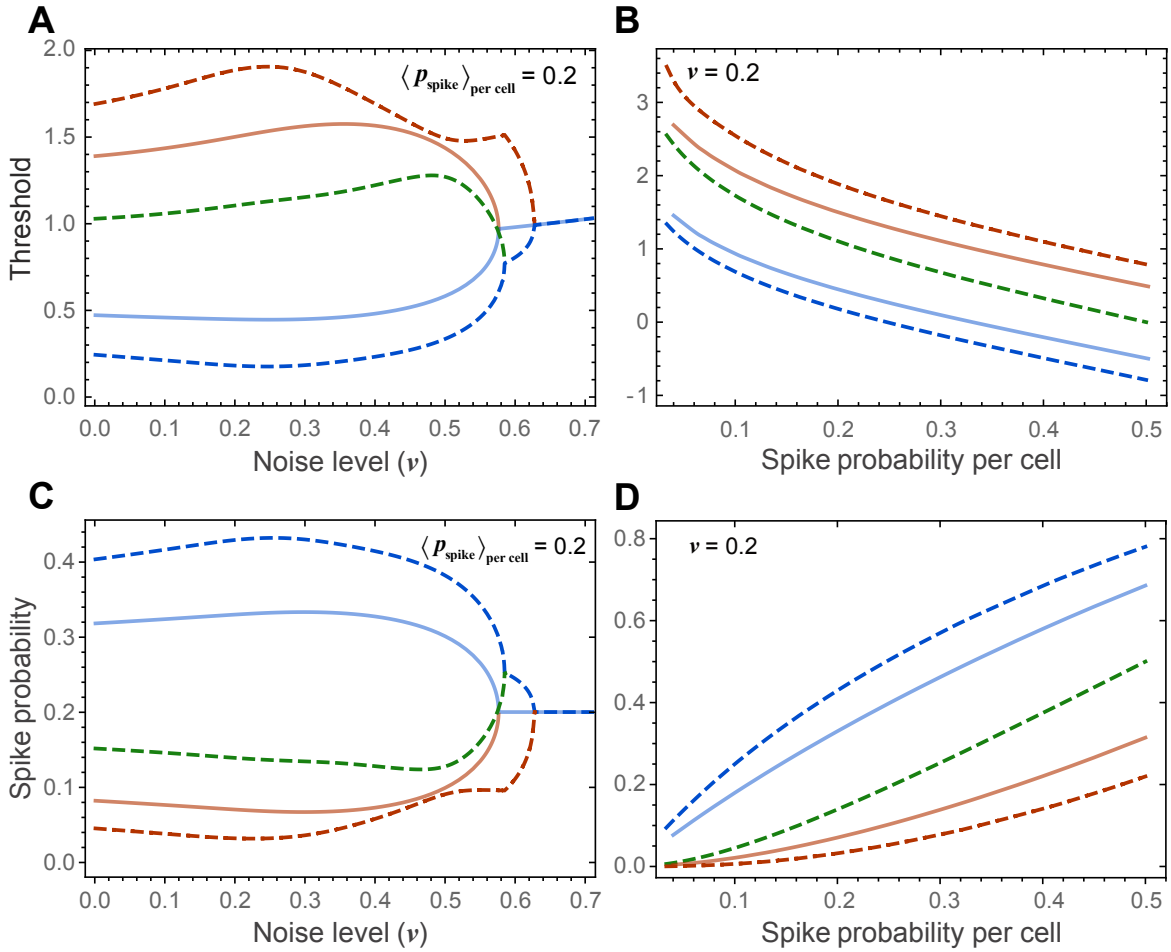

Figure 3.1: **Maximally informative solutions for a groups of neurons.** (**A**) The distribution of thresholds are plotted as a function of noise level ($\nu = \nu_1 = \nu_2$), but subject to a constant total spiking probability ($p_{spike} = 0.2$), for the two (solid-line) and three neurons (dashed-line). (**B**) is the same as (A) but shown as a function of total spiking probability (p_{spike}) subject to constant neural noise ($\nu_i = 0.2$). (**C**, **D**) are similar to (A, B) but shows the distribution of individual spiking probability in groups of neurons.

(μ_i, ν_i) onto that of $(p_{spike}, \mu_1 - \mu_2, \frac{\nu_1+\nu_2}{2}, \nu_1 - \nu_2)$, which is similar to what we demonstrated with the single-cell case (c.f. Sec. 2.2). This makes it possible to predict the optimal value for $\Delta\mu = \mu_1 - \mu_2$ via information maximization under the constraints (or knowledge) of other three parameters. Besides, one can test to what degree theoretical predictions agree with experimental data.

The most prominent feature of the mutual information is a bifurcation that occurs when noise decreases below a certain, critical value ν_c (Fig. 3.2). In the case where both neurons have

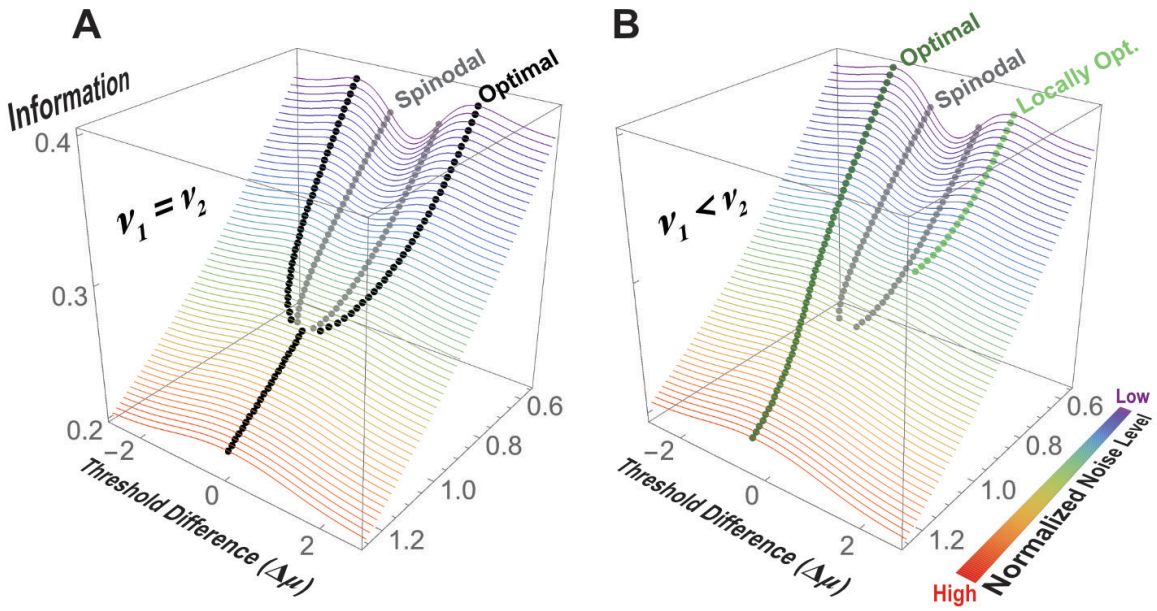

Figure 3.2: **Information predicts the optimal thresholds for a pair of neurons given the values of noise level.** (**A**) and (**B**) shows the information transmitted by a pair of neurons at different values of noise and thresholds. The noise level is the same for the two neurons in (**A**) and different in (**B**), $\Delta\nu/\nu_c = -0.02$, between neurons. Each colored curve is the information as a function of $\Delta\mu$ at a given mean noise level $\left(\nu = \frac{\nu_1+\nu_2}{2}\right)$. Black and dark-green dots mark global and local information maxima, respectively. Local maxima appear when noise levels differ across neurons (**B**); otherwise the maxima are equivalent as in (**A**). Gray dots mark the inflection points, the so-called spinodal lines that delineate the regions where local maxima can be found.

the same noise levels $\Delta\nu = 0$ ($\nu_1 = \nu_2$, Fig. 3.2 (A)), a single peak at zero threshold difference $(\Delta\mu)$ splits into two symmetric peaks upon decreasing the mean noise level (ν). Each of these peaks represents equivalent solutions obtained by exchanging neuronal indices. One of the peaks describes the case where $\mu_1 > \mu_2$ whereas the other describes the case where $\mu_1 < \mu_2$. When neurons have different noise values ($\nu_1 > \nu_2$), the peak with $\mu_1 > \mu_2$ is globally optimal while the other with $\mu_1 < \mu_2$ becomes suboptimal, and vice versa (Fig. 3.2 (B)). Thus, the lower threshold neurons should have lower noise. This agrees with the intuition that a neuron which is more sensitive to small input fluctuations should have smaller noise.

3.2.2 Test of maximally informative model in retina

One can test the predicted maximally informative solutions on the responses of pairs of retinal ganglion cells (RGCs) that encode the same temporal fluctuations of light intensities but with different thresholds [25]. These cells have been termed 'adapting' and 'sensitizing' based on their short-term plasticity, but for the present analyses in steady-state conditions, the main differences between these cell types are that adapting cells have higher thresholds and larger noise levels than sensitizing cells.

From the measurements of the average spike rate for two neurons (p_{spike}), one can predict the critical noise value (ν_c) below which one can expect to find neurons with different thresholds encoding the same filtered stimulus x. The measured noise values for the adapting and sensitizing retinal ganglion cells (RGCs) were indeed below the critical noise value (ν_c) [27]. This explains why these two separate cell types are observed among Off neurons but not among On neurons whose measured noise values are above ν_c [27]. In addition, one can make detailed predictions for the expected threshold difference ($\Delta\mu$) based on the measurements of other three parameters $\left(p_{spike}, \frac{\nu_1+\nu_2}{2}, \nu_1-\nu_2\right)$. Note that both the threshold difference ($\Delta\mu$) and critical noise (ν_c) depend on the average spike rate (p_{spike}) that changes from one to another cell pairs and under different stimulus condition. To show all the retinal data $\left(\Delta\mu, \frac{\nu_1+\nu_2}{2}\right)$ on one $x-y$-plane that is universal across different p_{spike}, we transformed the data based on the rescaling method provided in Ref. [27] . Here, theoretical predictions were in qualitative agreement with experimental measurements, but quantitatively the observed threshold differences between the adapting-sensitizing neuron pairs were systematically smaller than those predicted based on maximizing information (Fig. 4.8 (A)) [27].

Additional theoretical efforts indicate that including multiple noise sources could affect the predictions for threshold differences between cell types [11]. Therefore, in the next Chapter we address whether a model with multiple nonlinearly interacting pathways could quantitatively explain the existing RCG data on coordination thresholds between the two cell types.

Chapter 3, in part, have been submitted for peer review of the material as it may appear in Cell Reports, Hsu, Wei-Mien; Kastner, David B.; Baccus, Stephen A.; Sharpee, Tatyana O., Cell Press. The dissertation author was the primary investigator and author of this paper.

Chapter 4

The influence of threshold modulation on maximally informative encoding strategies

Previous chapters have covered the efficient nonlinear properties for a single and a group of neurons, regulated by different constraint settings. However, it is also important to consider the case where information transmission occurs in the presence of fluctuations in input statistics that might not be strong enough, or persist for long enough time, to trigger full-scale adaptation. These types of fluctuations are nevertheless important to take into account because they can evoke and/or represent modulatory influences from other circuits, as is ubiquitous in the brain. For example, modulatory influences include contextual or top-down signals about input properties on the scales larger than that of the neuron's primary receptive field, which closely follows the neuron's linear or the so-called classical receptive field [49]. Such contextual effects underlie figure-ground segmentation, motion selectivity, motion reversal or anticipation and other predictive effects in the retina the retina [20, 26, 24]. These effects are also prominent in the cortex where they include cross-orientation suppression [37, 39] and other non-classical receptive field effects in visual [45, 49] and auditory [6] cortices. Threshold modulation can also result from the direct action of neuromodulatory circuits [2] that represent changes in arousal

and attention [28, 34, 21]. The ubiquity of modulatory signals makes it essential to consider how they may influence the properties of maximally informative neural circuits.

Previous maximally informative solutions for pairs of neurons accounted for many aspects of these neurons' responses, including why these two separate cell types are observed among Off neurons but not among On neurons [27]. However, some noticeable quantitative differences between theory and experimental measurements were left unexplained [27]. Recent studies have pointed out that incorporating multiple noise sources could affect the predictions for threshold differences between cell types [11]. Therefore, we set out to determine whether modulatory effects on a cell's threshold would influence the theoretical predictions, bringing them into better agreement with experimental measurements. After testing a number of scenarios, we found that a model where a secondary pathway modulates the threshold of the primary pathway for each cell type (Box 4.1) could quantitatively account for the measurements of threshold differences between cell types, across several different contrasts. We envision that this threshold modulation occurs even for a fixed contrast, and in the case of the retina derives from contextual modulation from inputs on scales larger than neuronal receptive field center, or for cortical neurons, the classical receptive field [50].

4.1 Maximally informative model in the prescience of threshold modulation

Neural responses with threshold modulation

To understand information transmission in the presence of threshold modulation, once again, we modeled responses of individual neurons as binary, 1 or 0, corresponding to the presence or absence of a spike in a small time bin, respectively (Sec. 2.1). This model of neural responses yields a saturating nonlinearity shown in Box 4.1 and described by the following

Box 4.1 Two-pathway model of information transmission in the presence of threshold modulation

Schematic of the two pathway model with modulation

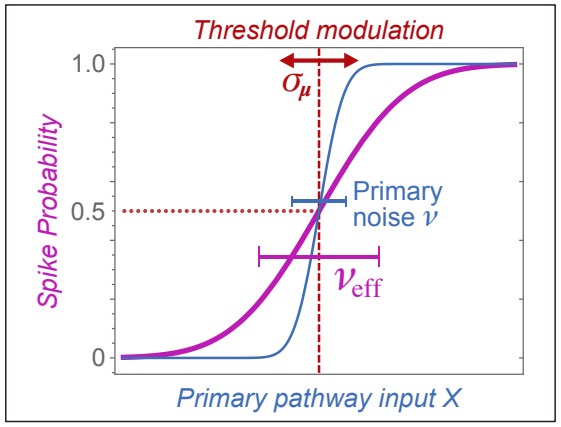

Measured variation in nonlinearity parameters

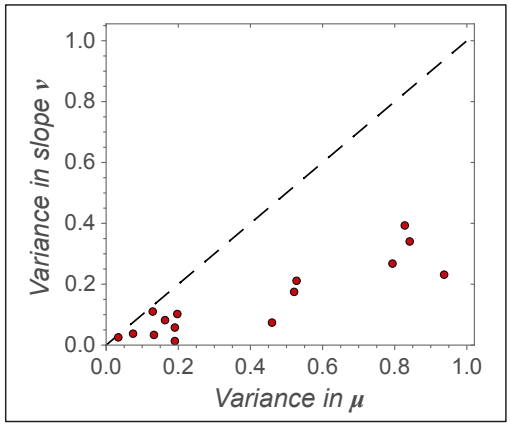

The experimentally observed neural nonlinearity reflects two noise sources:

- the intrinsic noise ν in the primary pathway
- threshold modulation that occurs on longer time scales with variance σ_μ.
- Over time, the observed nonlinearity is an average over different threshold positions $p(r|x) = \int d\tilde{\mu} p(r|x,\mu,\nu) p(\tilde{\mu})$ and has an effective width $\nu_{\text{eff}} = \sqrt{\nu^2 + \sigma_\mu^2}$.
- Right panel: Threshold variation over time is much stronger than variation in the primary noise.

Figure 4.1: Two-pathway model of information transmission in the presence of threshold modulation.

equation:

$$p(r=1|x,\mu,\nu_{\text{eff}}) = \frac{1}{2}\left[1 + \text{erf}\left(\frac{x-\mu}{\sqrt{2}\nu_{\text{eff}}}\right)\right]. \tag{4.1}$$

In this equation, we write ν_{eff} instead of ν to emphasize the fact that the observed noise in neural responses represents actually a joint effect of multiple different types of noise [11]. Here, we will focus on two types of noise: the "primary" noise ν that arises in the direct afferent circuitry for each cell, and the secondary source of variability that arises from the modulation of the threshold μ of the primary pathway and acts on longer time scales. On short time scales, similar to those of the spike generating process, the threshold value does not vary, and variability in

neural responses is described by ν only. On long time scales ($\sim$ seconds) , which are necessary to measure the neural input-output function, its width is described by

$$\nu_{\text{eff}} = \sqrt{\nu^2 + \sigma_\mu^2}, \tag{4.2}$$

We note that, in principle, noise ν in the primary pathway can itself also be subject to modulation, not just the threshold μ. This modulation would also increase ν_{eff}. However, in practice, we found that variation in ν was much weaker (Box 4.1, right panel). Therefore, in what follows, we focus on the effect of modulation on changes in the threshold.

Mutual information with threshold modulation

To analyze the impact of threshold modulation on information transmission, we compute the mutual information in two steps:

1) On short time scales, mutual information between is computed for a fixed threshold μ:

$$I(\mathrm{X};\mathrm{R}|\mathrm{M}=\mu) = \sum_r \int dx\, p(r|x)\; p(x) \log_2 \frac{p(r|x)}{p(r)}, \tag{4.3}$$

where x is the filtered stimulus according to the spatiotemporal receptive field of the neuron, and $r \in \{0,1\}$ represents the response of a single neuron before the incorporation of the modulation in the secondary pathway ($\sigma_\mu = 0, \nu_{\text{eff}} = \nu$).

2) On longer time scales, we average the mutual information over the varying threshold value $\tilde{\mu}$:

$$I_{\text{long-term}} = \int d\tilde{\mu} I(\mathrm{X};\mathrm{R}|\mathrm{M}=\tilde{\mu})\, p(\tilde{\mu}). \tag{4.4}$$

Here, $p(\tilde{\mu})$ describes the distribution of threshold values.

The information in Eq. (4.4) is actually the so-called conditional mutual information [12]

$I(\mathrm{X};\mathrm{R}|\mathrm{M})$ between the input and the responses of the primary pathway, conditional of the signals μ from the modulatory pathway. As such, this information differs from the full information provided jointly by modulatory and primary pathways only by the term $I(\mathrm{X};\mathrm{M})$: $I(\mathrm{X};\mathrm{R}|\mathrm{M}) = I(\mathrm{X};\{R,\mathrm{M}\}) - I(\mathrm{X};\mathrm{M})$, where $I(\mathrm{X};\mathrm{M})$ represents information provided solely by the modulatory pathway. Because $I(\mathrm{X};\mathrm{M})$ does not depend on the parameters of the nonlinearity of the primary pathway, it can be dropped when searching for the maximally informative properties of the primary pathway. Thus, one can find the maximally informative setting for the primary pathway and the optimal modulation by maximizing information from Eq. (4.4). These arguments generalize to the case of multiple neurons where one evaluates information between inputs X to the primary pathway of each neuron and the vector of responses across the neural population $\mathbf{R} = \{r_i\}$, $r_i \in \{0,1\}$.

4.2 Impact of threshold modulation on information transmission

We start by considering the impact of threshold modulation on single neurons. Here, modulation always decreases information transmission (Fig. 4.2 (A)). However, for an equivalent amount of variance, modulation decreases information less than does primary noise. Therefore, if the system has a choice between reducing the primary noise or reducing modulation, it is always preferable to reduce the primary noise first, cf. Fig. 4.2 (B).

The effect becomes more interesting in groups of neurons, starting with pairs of neurons. Here, we find that if modulation is directed to the neuron with the lowest firing rate in the group, then the negative effect of modulation is almost completely removed, cf. Fig. 4.3, panels (A) and (B). In these calculations, the firing rates were assigned to maximize information while constraining the average spike rate across the neurons (Fig. 4.4). We find that one can apply much larger modulation to a single neuron than the modulation distributed to many neurons and

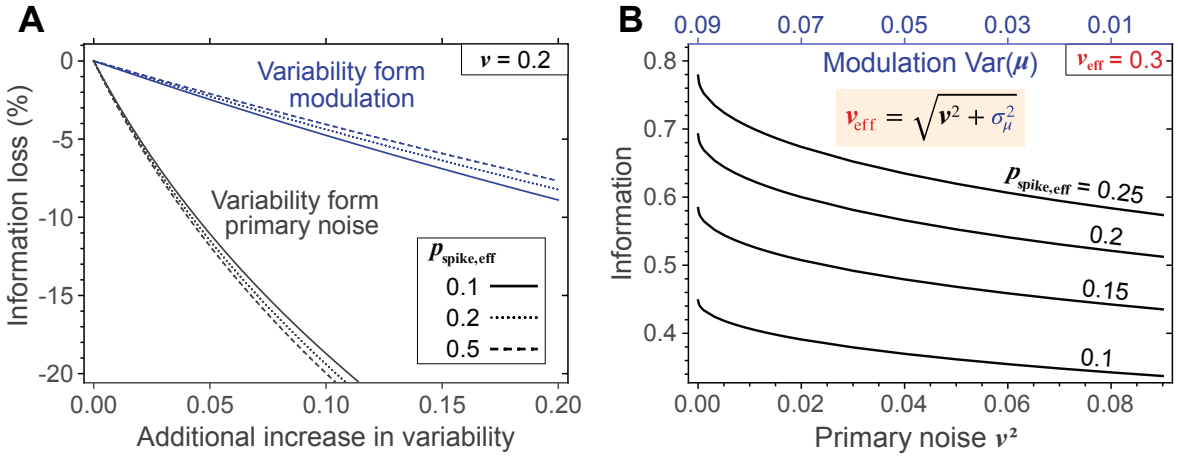

Figure 4.2: **Impact of threshold modulation on information transmission.** (**A**) The difference in information before and after adding different types of variability: either modulation (blue lines) or primary noise (black lines). Both of types of variability decrease information, but modulation (blue lines) decreases information much less than the primary noise (black lines). We note that both the primary noise and the modulation also increase the spike rate. Therefore the baseline information (without modulation) is computed for the higher rate that matches the rate in the presence of modulation. (**B**) The stronger detrimental effects of primary noise on information transmission compared with modulation are shown here for the case where primary noise and modulatory variance are constrained to sum $\nu_{\text{eff}} = \sqrt{\nu^2 + \sigma_\mu^2} = 0.3$. In this case, the smaller the primary noise (bottom x-axis), the larger the information (y-axis), despite the corresponding increases in modulatory variance (top x-axis).

still have less of a decrease in information. Selective application of modulation also maximized information in groups of three neurons (Fig. 4.3 (C, D)). With three neurons, information was maximally preserved under modulation when it was applied to the neuron with the smallest spike rate. The most detrimental effects of modulation were observed when modulation was applied to the neuron with the largest spike rate. This was followed by progressively better results if modulation was applied equally to all neurons or to the neurons with the intermediate spiking rate. However, these intermediate cases still led to worse performances compared to the case where modulation is directed to the neuron with the lowest spike rate (Fig. 4.3D). The degree of protection from modulation-induced loss is higher for the three-neuron circuit compared with a two-neuron circuit (Fig. 4.3 (D)). This suggests that the benefits of including a sparsely responding neurons can be larger in large groups of neurons.

We also examined the case where neurons have the same thresholds and spike rates, as can be optimal for high values of the primary noise [27]. In this case we found that the optimal ways to apply modulation differed depending on whether same-threshold neurons had small or large spike rates, cf. Fig. 4.5. In the case where neurons had small rates, it was optimal to apply modulation equally to both of them. In the case where neurons had large response rates, it was optimal to direct modulation to one of the neurons than split it equally to both neurons (Fig. 4.5). The application of modulation lowered the spike rate in the target neurons. The implication from these results therefore is that if a large neural circuit contains neurons of the same type with small spike rates, such as for example the adapting cells in the retina, then modulation should be applied selectively to the class of neurons with sparse responses and equally within this class neurons.

Why is it beneficial to direct modulation to the neuron with the lowest spike rate? An intuitive explanation for this phenomenon can be obtained by considering the shape of the information function for a single neuron with respect to its threshold (Fig. 4.6 (A)). This function is concave for small thresholds and convex for large thresholds. This is important because concave functions decrease their value upon averaging of their inputs, as occurs as a result of threshold modulation, while convex functions increase their value. This means that neurons with small thresholds, i.e. high spike rates, will suffer a decrease in information transmission upon modulation, cf. Fig. 4.6 (B). In contrast, neurons with large thresholds, i.e. small spike rates, will increase information transmission upon threshold modulation. The lower the spike rate, the greater is the increase in the information transmission with modulation.

At this point, it is important to clarify that this increase in information transmission with modulation is accompanied by an increase in the spike rate. Unlike information, the firing rate function is convex for all values of its argument (Fig. 4.6 (A)). As a result, modulation always increase the spike rate (Fig. 4.6 (C)). The increase in the information from modulation is less than it would have been if the rate was simply increased by lowering the threshold, without the

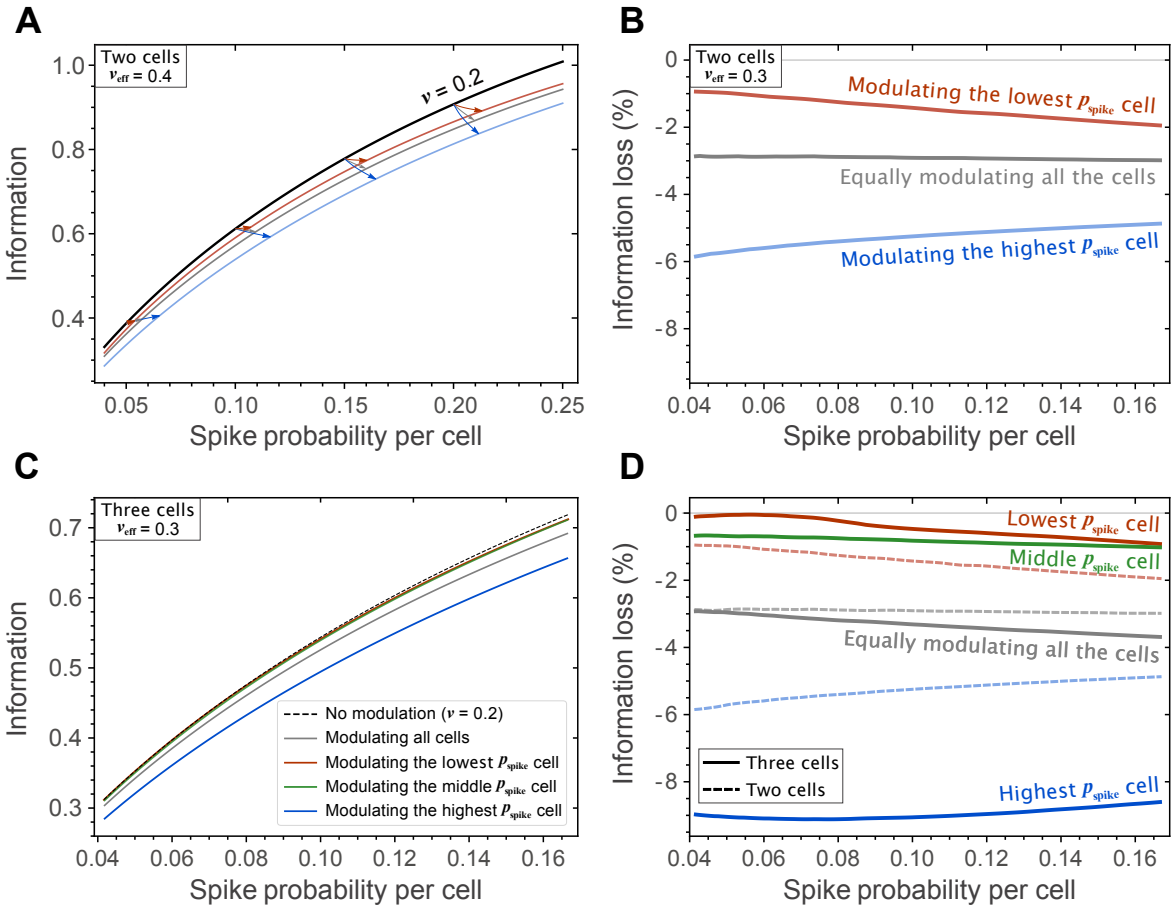

Figure 4.3: **Modulation directed to sparsely responding neurons protects against information loss in the presence of modulation**. (**A**) The information loss is smallest when only the lowest-spiking neuron (red line) receives modulation, compared to modulating all neurons (gray line) or the highest-spiking one (blue line). Black line shows information in the absence of modulation. The primary noise $\nu = 0.2$ for all cases, lines with modulation have the same averaged effective noise $\nu_{\text{eff}} = 0.4$ after modulation. Arrows describe how points on the unmodulated curve change in terms of information and spike rate upon adding the same amount of overall modulation. The red and blue arrows have different final values for spike rate because the modulation-induced increase in the spike rate depends on the initial spike rate values and is different for the lowest and highest spiking neuron in the pair. The averaged effective noises after modulation are $\nu_{\text{eff}} = 0.3$ for all curves. The spike rates were optimized to yield maximal information for a given average spike rate. The corresponding rates are shown in Fig. 4.4. (**B**) Same as (A) but in terms of percentage of information loss to show the results on an expanded scale. (**C, D**) Same as (A) and (B) but for three neurons. In (**D**), results from (B) pertaining to pairs of neurons are re-plotted using dashed lines for comparison. Green lines shows the case where modulation is directed to the neurons with intermediate spike rates, other colors are the same as for pairs of neurons. Directing modulation to the most sparse neurons yields the smallest information loss from modulation. Modulation can be more fully compensated in three-neuron groups compared to two neurons, for smaller spike rates.

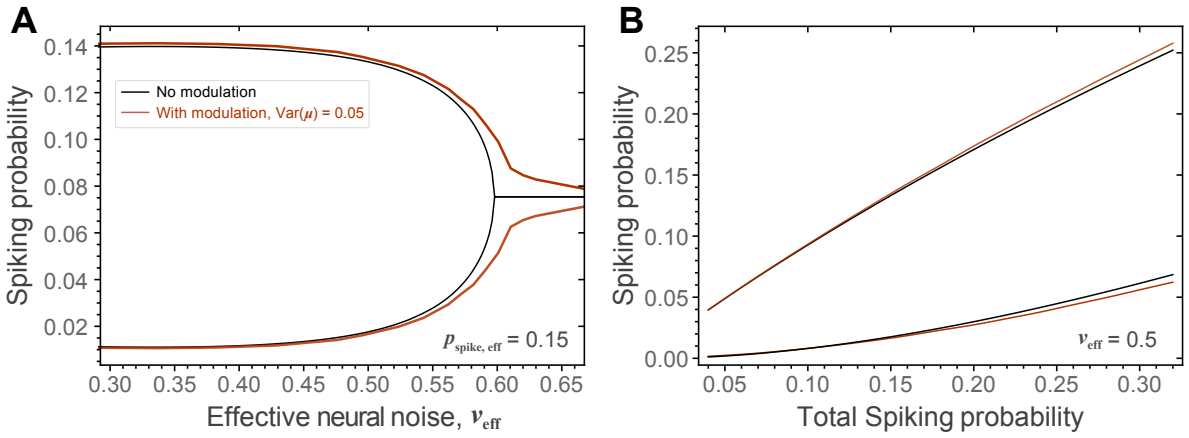

Figure 4.4: The maximally informative spike rates among neurons were similar for models with and without threshold modulation. The results shown here correspond to the analyses of the impact of threshold modulation shown in Fig. 4.3.

modulation. As a result, the information vs. rate curve in the presence of modulation has the same shape as in the absence of modulation, just with reduced information for a given rate.Thus, these results are consistent with those in Fig. 4.2 (A) showing modulation decreases information. It is just that the increase in information upon modulation can nearly completely match the increase that would have been observed if the firing rate was increased without modulation.

The conclusions from the theoretical analyses of information transmission in the presence of threshold modulation indicate that modulation should not be equally distributed to all neurons in the target circuit. Instead, it should be directed to the neuron with the lowest spike rate with inhibitory signals. The use of inhibitory signals ensures that the rank-ordering of neurons does not change under modulation, and the neuron that receives modulation does not get its spike rate raised. They also illustrate the need to use neurons with diverse spike rates, because the average spike rate in the circuit sets the upper limit on the amount of information that this group of neurons can transmit, with or without modulation. To have the capability to transmit large amounts of information, the circuit has to include neurons with large spike rates. Including neurons with small response rates and directing modulation to them helps maintain information transmission near its maximal levels in the presence of modulation.

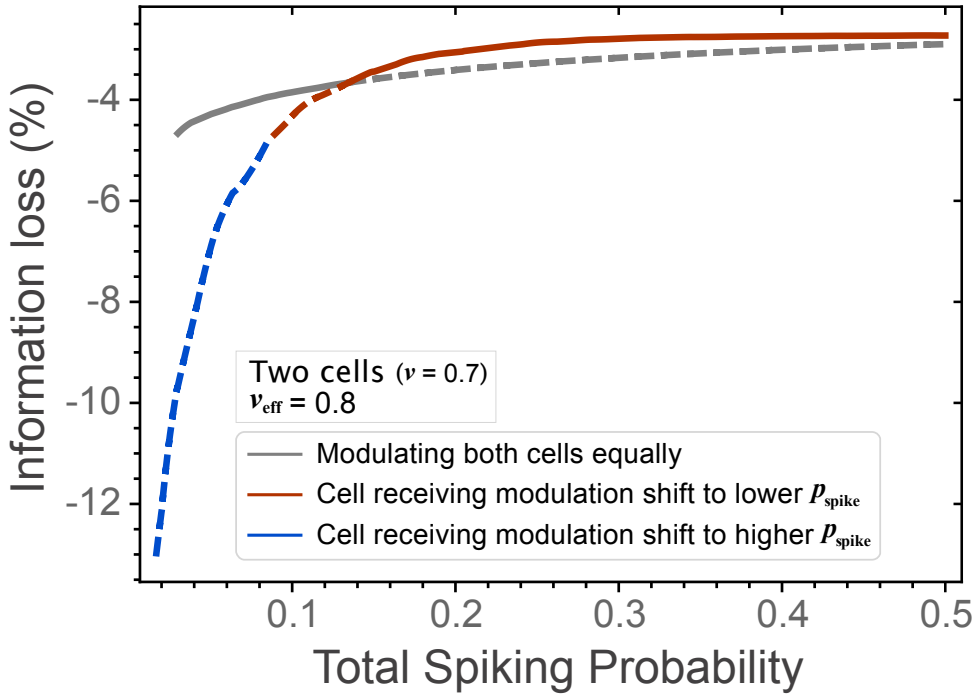

Figure 4.5: **Optimal ways to apply modulation for neurons with identical spike rates depend on their rates.** For neurons with low spike rates, the negative impact of threshold modulation is minimized when modulation is applied equally to both neurons (gray line). For neuron with large response rates, selective application of modulation to one of the neurons is preferred. The neuron receiving modulation shifts its threshold to decrease its response rate (red line). Curves are shown as dashed in the regimes when they become sub-optimal in terms of information transmission in the presence of threshold modulation.

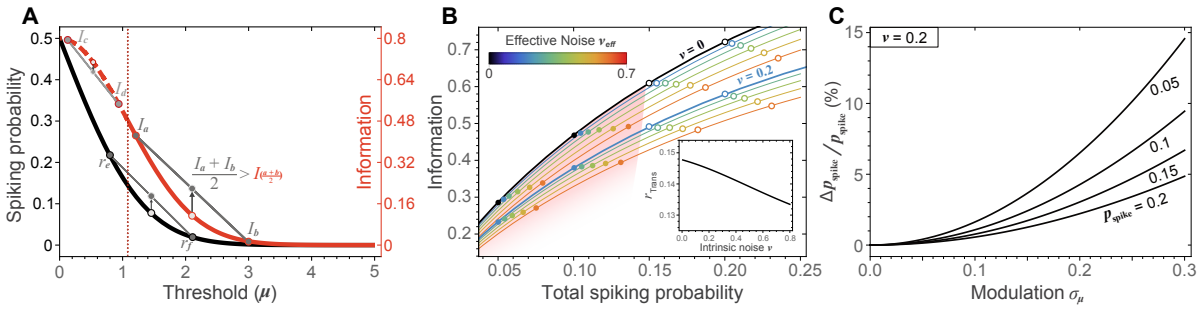

Figure 4.6: **Modulation induced transition in information transmitted as a function of spike rate.** (**A**) Spike probability is a convex function of threshold position (black line). In contrast, information (red line) changes convexity as a function of threshold. When a function has positive convexity (solid segments of the curve) the average of its two values at points a and b is always larger than the function value at $(a+b)/2$. In this regime, fluctuations increase information transmission. The opposite is true for regions of negative convexity (dashed-curve). As a result, fluctuations in threshold decrease information when thresholds are low and increase information when threshold are high, i.e. when neurons respond sparsely (**B**) Threshold modulation increases information transmission when spike rates are small (filled dots) but decreases it when spike rates exceed a certain transitional value (open dots). Shaded pink region denotes the value where modulation increases information transmission. Thick solid lines show information in the absence of threshold modulation ($\sigma_\mu^2 = 0$), for two noise levels $\nu_{1,2} = 0$ (black) and 0.2 (light-blue). Thin solid lines and the eight series of color-dots on them show how curves shift upon introduction of threshold modulation. Each series of color-dots evolves from the same intrinsic noise (ν) and threshold (μ). Color denotes the resulting effective noise $\nu_{\text{eff}} = \sqrt{\nu^2 + \sigma_\mu^2}$. (**Inset**) The transitional value in response rate is plotted as a function of the intrinsic noise. (**C**) Modulation increases response rate.

4.3 Test of maximally informative prediction in the presence of threshold modulation

4.3.1 Retinal input-output functions are maximally informative under threshold modulation

We now test how these predictions using responses of pairs of cells in the retina that differ in their average spike rates. The adapting and sensitizing cells are two cell types that represent the same temporal pattern of light intensity modulation but have different thresholds. Our first analysis is to fit the maximally informative model with modulation to the responses of pairs of adapting/sensitizing cells. The fit was made while requiring that the effective noise and the average spike rate for the pair matched experimental measurements (see Appendix D for details). The fit yields estimates for threshold modulation and primary noise for each neuron in the pair as well as an estimate for the difference in their thresholds. These estimates can then be compared to direct experimental measurements of these variables.

We find that the inferred amount of noise in the primary pathway was similar for both adapting and sensitizing cells (Fig. 4.7 (A)). However, the threshold modulation was substantial for adapting cells and very close to zero for the sensitizing cells (Fig. 4.7 (A)). The fitting results were consistent across cell pairs. (Table D.1). Thus, the differences in the effective noise that are observed between these two cell types [25] are due to differences in threshold modulation. We also note that threshold modulation was small in sensitizing cell even relatively to their thresholds (the modulation was ~ 100 times smaller for sensitizing cells compared to adapting cells, whereas their thresholds are only approximately half as small as those of adapting cells).

The threshold modulation values predicted by the maximally informative model with modulation can be compared with direct experimental estimates of their threshold modulation. To compute the amount of threshold modulation that is observed experimentally, we estimated

neuronal nonlinearities from shorter data sub-sets (1/4 to 1/6 compared to the full dataset). Each nonlinearity was fit with a logistic function to determine its threshold value. We find that the observed variation in thresholds for a given adapting cell matches those estimated using the maximally informative model (Fig. 4.7 (B), paired non-parametric t-test $p = 0.73$). [This analysis was only carried out for adapting cells, because threshold modulation was negligible in sensitizing cells]. Those adapting cells that had larger variance in thresholds across trials also had larger values of threshold modulation as indicated by fitting the maximally informative model to the full set of their response (the correlation was statistically significant, with $p = 0.015$, Fig. 4.7 (B)). These analyses add credence to the use of the maximally informative model with modulation as a method for separating the noise component that is due to threshold modulation. They also indicate that the observed threshold modulation in adapting cells is maximally informative given their other parameters, such as the primary noise and firing rate.

Another prediction that one can obtain from the maximally informative model with modulation pertains to the differences in the thresholds between adapting and sensitizing cells. Previous predictions for the threshold differences obtained for pairs of neurons without taking modulation into account yielded values that were systematically larger than those observed experimentally [27], replotted in Fig. 4.8 with black line. We find that the maximally informative model with modulation provided more accurate predictions for thresholds differences between pairs of neurons than the model with no modulation, cf. Fig. 4.8. Statistically, the threshold difference (in units of contrast) between adapting and sensitizing cells were consistent between the average values across contrasts for each cell pairs from the maximally informative model and experimental measurements (paired non-parametric t-test $p = 0.14$). By comparison, the model with no modulation yielded systematically greater threshold differences that is observed experimentally (black line in Fig. 4.8). We note that experimental data points show larger residual variation across different contrasts than our model indicates. The reason for this is that, in the model, noise components and threshold modulation for adapting cells were constrained to

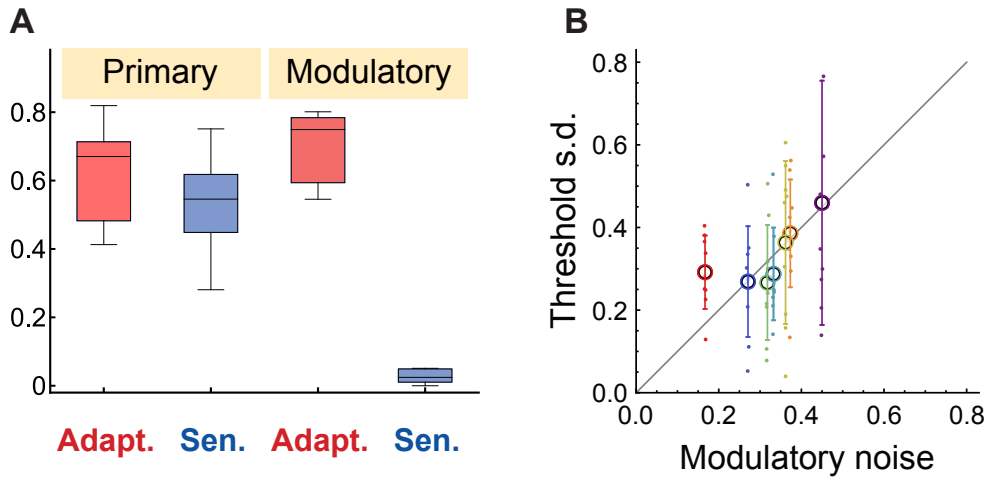

Figure 4.7: **Experimentally observed threshold variation matches maximally informative values.** (**A**) Intrinsic neural noise and threshold modulation inferred using the maximally informative model with modulation from retinal data. Both neural types have comparable amounts of intrinsic neural noise (ν_i) but distinct levels of threshold modulation ($\sigma_{\mu,i}$). All noise types varied linearly with the stimulus contrast, except for modulatory noise in the sensitizing cells, which was small and contrast-independent. (**B**) The experimentally observed threshold variation across adapting cells is positively correlated with threshold modulation inferred from the maximally informative model ($r = 0.3$, $p = 0.015$). Both axes are in units of contrast. Colors denote different neurons. Data points for the same neuron/color represent measurements from different input contrasts.

change linearly with contrast (to reduce the number of fitted parameters, see Methods). Thus, the model was not meant to predict residual variation across contrasts that remains after rescaling inputs by their contrast. Other than this variability, the predictions of the maximally informative model with modulation for threshold differences between adapting and sensitizing cells are fully consistent with experimental measurements (Fig. 4.8B).

4.3.2 Amacrine cells as a source of threshold modulation for adapting cells

One of the key predictions of the theory is that modulation should be directed to neurons with low spike rates. However, as we have seen above, modulation increases the spike rate (Fig. 4.6C), albeit by moderate amounts. One way to minimize the risk of altering the rank-

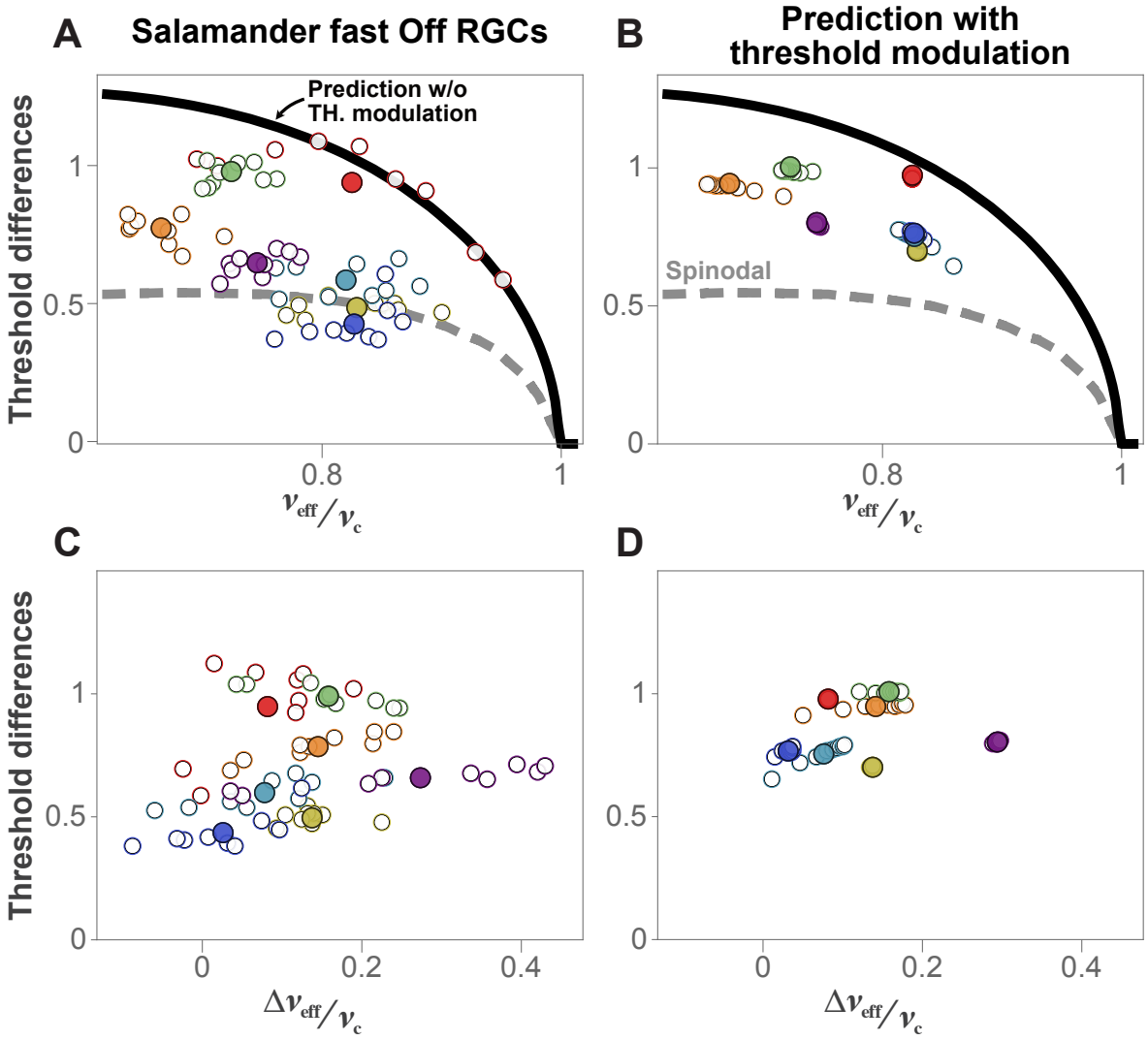

Figure 4.8: **Maximally informative model with modulation accounts for threshold differences between adapting and sensitizing cells.** Threshold difference between adapting and sensitizing cells is plotted as a function of average (top row) and difference (bottom row) in the effective noise between the two neurons. Columns show data (left), maximally informative predictions with modulation (right). Different colors denote different cell pairs. Open circles represent data for a given contrast, filled circles show the average across contrasts. Black lines show predictions for threshold differences without threshold modulation. Gray dashed lines denote spinodal lines that separate regions where information has two maxima vs. a single maximum. Points close to the spinodal lines (e.g. blue, light blue, and light green) are more difficult to fit because they mark the region where one of the maxima ceases to exist. This pushes the interpolated solutions away from the spinodal line (c.f. Fig. 3.2). Despite these technical issues, the overall distribution of mean threshold values normalized across contrasts was not statistically different between fitted and experimental values, $p = 0.14$.

ordering of neurons in terms of their spike rate is to deliver it with inhibitory neurons. In this way the neuron that is undergoing modulation will automatically have its threshold raised and spike rate lowered. This is consistent with our observations in the retina where adapting neurons, which undergo modulation, also have larger thresholds and smaller spike rates. In the retina, inhibitory amacrine cells could be the source of that input (Fig. 4.9A). If amacrine cells provide stronger inputs to adapting cells than the sensitizing cells, then this would simultaneously explain why the thresholds of adapting cells are higher and more variable than those of sensitizing cells. The fact that both the mean threshold and its modulation varies approximately linearly with contrast is also consistent with this wiring scheme. Inputs to and from amacrine cells just need to be scaled by contrast just like inputs within the primary pathway for the adapting and sensitizing cells.

We tested this hypothesis by performing a separate set of experiments to analyze how the hyperpolarization and depolarization of sustained Off-type amacrine cells by intracellular current injection affected responses of nearby adapting and sensitizing cells recorded simultaneously with a multielectrode array (see Methods and Fig. 4.9). Specifically, we analyzed the change in the mean threshold of adapting/sensitizing neurons between hyperpolarization and depolarization of the amacrine cell. When an amacrine cell is hyperpolarized (depolarized), this decreases (increases) its inhibition onto neurons it is directly connected to. Although we do not assume that there are direct connections between amacrine cells and the ganglion cells we recorded (the connection could be polysynaptic, through circuitry involving bipolar or other amacrine cells), this approach measures the functional effect of individual amacrine cells. In Fig. 4.9C we plot the change in the threshold as a function of distance between the receptive fields (RFs) of the amacrine cell (that was subjected to hyperpolarization/depolarization) and the adapting/sensitizing cell whose nonlinearity was measured to estimate its threshold. In the case of adapting cells, there was a clear and statistically significant dependence of the amount of threshold shift as a function of the distance to the amacrine cell RF center ($p = 8 \times 10^{-5}$

F-test compared with null hypothesis of no dependence on distance). The dependence was not statistically significant in the case of sensitizing cells ($p = 0.9$). Thus, these data support the hypothesis that the larger thresholds of adapting ganglion cells arise as a result of inhibition from the amacrine cells, and that this inhibition also brings with itself stronger threshold modulation.

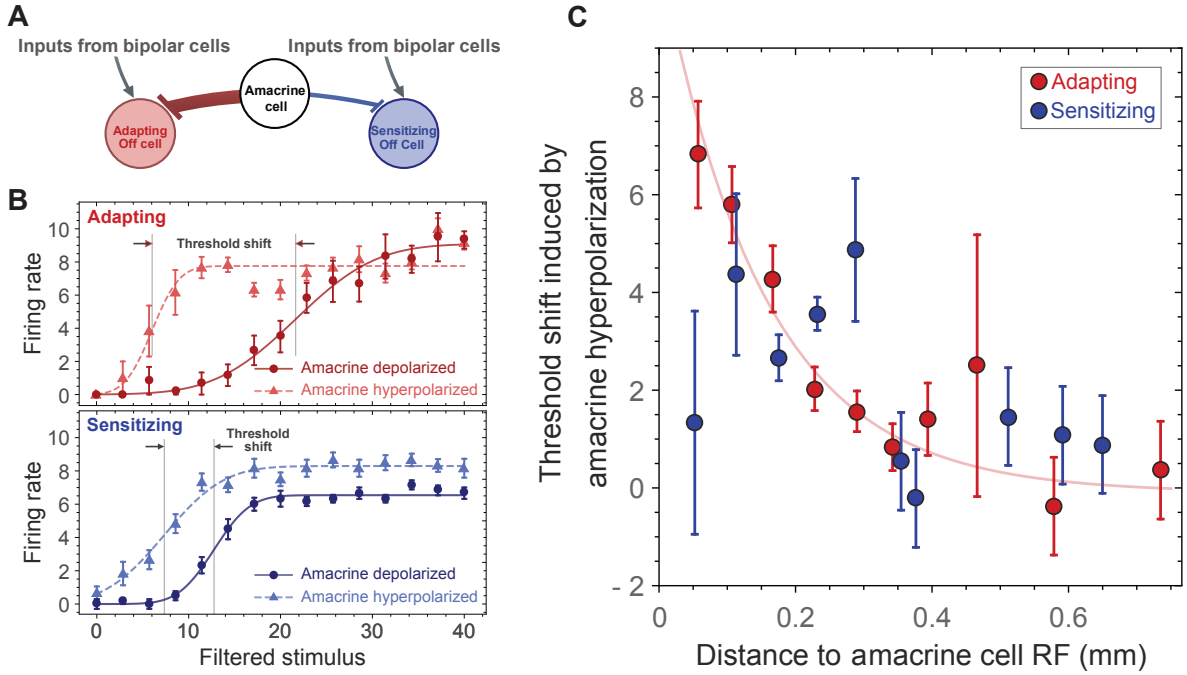

Figure 4.9: **Distance dependent inputs from amacrine to adapting cells.** (**A**) Inferred model of the presynaptic circuitry of the two types of Off retinal ganglion cells based on observed differences in the strength of the modulatory pathway. (**B**) The nonlinearity of Off ganglion cells during the depolarizing (dot) and hyperpolarizing (triangle) current injection into the amacrine cell. The solid and dashed curves show the fit with sigmoid function. The distance between the receptive field (RF) of the amacrine cell to that of the adapting cell was 0.090 mm, 0.101 mm to the RF of the sensitizing cell. (**C**) The amount of inhibitory input from amacrine cells to the adapting cell decreases with distance significantly ($p \times 10^{-8}$, f-test). [Inhibition may be direct or polysynaptic, through circuitry involving bipolar cells or other amacrine cells.] The dependence on distance was not statistically significant for sensitizing cells ($p = 0.9$). Solid lines show the exponential fits with distance.

4.4 Conclusion

In this work we analyzed information transmission in the presence of threshold modulation. There are two main conclusions. The first conclusion is that modulation should not

be equally applied to all neurons in the circuit. Instead it should be directed to select neurons, preferably those with the low spike rates in the circuit. The second conclusion describes the central role that inhibitory neurons play in delivering modulatory signals into the circuit. These conclusions are obtained by through basic analyses using information theory, and therefore should apply to all neural circuits. We now discuss the implications of these conclusions, with a focus on cortical circuits.

The first conclusion highlights the need to form circuits using neurons with different spike rates. The large number of sparsely firing neurons in the cortex have long presented a puzzling observation [41]. The chief explanation offered so far is that sparse response reflect due to metabolic constraints. However, one could have hypothetically used a smaller number of neurons with higher spike rates, if metabolic constraints were the leading cause for the sparseness of neural responses. The information-theoretic analyses in the presence of modulation offer a different explanation. Neural circuits need to have neurons with both high and low firing rates in order to transmit large amounts of information in the presence of modulation. High firing neurons make it possible to transmit large amount of information, whereas neurons with small spike rates protect against loss of information transmission in the presence of modulation.

The second conclusion describes a rather unexpected role for inhibitory neurons as intermediaries for delivering modulation signals. This set up helps to ensure that low-spiking neurons that receive modulation remain in this regime under varying modulation levels. We find support for this prediction in the retina where inhibitory amacrine cells send modulatory signals to sparsely spiking adapting cells. If modulation were delivered to adapting cells via excitatory pathway, then this would risk making their spike rate greater than that of sensitizing cells and losing protection against negative effects of threshold modulation on information transmission.

The same role appears very plausible for inhibitory neurons in the cortex. There, inhibitory neurons expressing the vasoactive intestinal peptide are the major target of neuromodulatory inputs as well as modulatory, context-dependent inputs from higher-order cortical

areas [23]. Similarly, somatostatin expressing inhibitory neurons use this neuropeptide as a co-transmitter with GABA to modulate the activity of local neurons [32, 48]. The slow action of neuropeptides, such as somatostatin, conforms with our modeling framework where modulation changes neuronal threshold on slower time scales than those on which the primary activation pathway operates. We note also that all of the other inhibitory neurons, including parvalbumin-positive inhibitory neurons, are directly responsive to neuromodulators such as acetylcholine and serotonin [52]. Furthermore, even when neuromodulators, such as acetylcholine, act directly on excitatory neurons, they exert first an inhibitory response [14] in their target neurons. The information-theoretic results offer a new explanation for this tight link between neuromodulatory and inhibitory circuits in the brain.

Chapter 4, in full, have been submitted for peer review of the material as it may appear in Cell Reports, Hsu, Wei-Mien; Kastner, David B.; Baccus, Stephen A.; Sharpee, Tatyana O., Cell Press. The dissertation author was the primary investigator and author of this paper.

Appendix A

Data acquisition

A.1 Experimental preparation

We use a combination of new and previously published experimental data [25]. Full details of the experimental procedures for measuring neural nonlinearities are provided in [25]. Briefly, uniform field stimuli were drawn from a Gaussian distribution with constant mean intensity, M, of 10 mW/m^2. Contrast is defined as $\sigma = W/M$, where W is the SD of the intensity distribution. Neurons were probed with flashes of nine different contrast values from 12% to 36% in 3% intervals. The contrasts were randomly interleaved and repeated. Each contrast was presented, in total, for ≥ 600 s. For the calculation of the response functions, the first 10 s of data in each contrast were not used to allow for a better estimation of the steady state.

A.2 Intracellular recording

Simultaneous intracellular and multielectrode recordings from the isolated intact salamander retina were performed as described [35]. Sustained amacrine cells were distinguished from horizontal cells by their flash response and their spatiotemporal receptive fields, with

horizontal cells lacking an inhibitory surround and being greater than 300 μm in diameter. For the intracellular recordings the stimulus comprised of randomly drawn contrasts with contrast amplitudes that ranges from 0 to 40% Michelson contrast units, where Michelson contrast is defined as $(I_{\max} - I_{\min}) / (I_{\max} + I_{\min})$. The flash amplitude varied randomly every 400 ms, the first 100 ms the flash was greater than the mean, from 100 to 200 ms the flash was lower than the mean, and for the last 200 ms the flash was at the mean luminance level. Changing the distribution of amplitudes slower than the integration time of ganglion cells allowed for a rapid measurement of the ganglion cell response function without having to also measure the ganglion cell temporal filter [9]. Synchronized to the visual stimulus, we injected from 100 to 300 ms, randomly interleaved, hyperpolarizing (-500 pA) or depolarizing ($+500$ pA) current pulses into the amacrine cell. The ganglion cell response function was calculated at the firing rate of the ganglion cell from 100 to 400 ms of each contrast amplitude. This focused on the off response of the ganglion cell.

A.3 Analysis of inhibition from amacrine cells versus RFs distance

To quantify the amount of inhibition from the amacrine cells to a ganglion adapting/sensitizing cells (Fig. 4.9), we analyzed how the threshold of the ganglion cells changes when nearby amacrine cells are depolarized or hyperpolarized. For each ganglion cell and amacrine cell condition, the relation between firing rate and filtered input was recorded (c.f. Method of intracellular recording). Fitting the two response curves with sigmoid functions yielded thresholds of a ganglion cell during the hyperpolarizing (μ_{h}) and the depolarizing (μ_{d}) current injection to the amacrine cell. The difference in thresholds ($\mu_{\mathrm{d}} - \mu_{\mathrm{h}}$) reflects the impact of amacrine cell inputs on the response properties of the ganglion cell. We analyzed these differences as a function of the receptive field distance between the ganglion and amacrine cells. Overall, the

analysis was based on current injection to 40 different amacrine cells and recordings from 144 Off ganglion cells. We note that an amacrine cell usually connects to multiple ganglion cells, and some of the ganglion cells receive inputs from multiple amacrine cells. The red and blue points shown in Fig. 4.9 are obtained by binning (according to RFs distance) results from 169 amacrine-to-adapting cell pairs and 32 amacrine-to-sensitizing pairs, respectively. The standard error in RFs distance (x-axis error) is too small to be visible in the plot.

Appendix B

Impact of threshold modulation on maximally informative threshold positions

To understand how threshold modulation affects maximally informative threshold positions, one may note that threshold modulation effectively smooths the information surface computed over long time scales (Fig. B.1). In the regime where the mutual information has two maxima, it has the effect of bringing the maxima closer to each other. Another effect that proved necessary to take into account is that noise in the primary pathway can be larger for the neuron that experiences smaller threshold modulation, leading to a smaller overall effective noise value for that neuron. In this case, the information transmitted matches the smaller (local) of the two maxima of the information. In other words, the model allows for the possibility that coordination of neural thresholds between neurons might not be able to keep up with changes in input statistics for the circuit to match the properties of the global maximum of information. Instead, we observed that in some cases neural response properties match a local maximum of the information that required smaller adjustments in thresholds following the change in input statistics.

Taking both of these effects – threshold modulation and the possibility of local optimality

– made it possible to account for the observed threshold differences between sensitizing and adapting cells. Each cell pair was probed with flashes of nine different contrasts, producing four experimental parameters of the neuronal nonlinearity ($\nu_{\text{eff},1}$, $\nu_{\text{eff},2}$, μ_1, μ_2) at each contrast. The maximally informative model also has six parameters (μ_1, μ_2, ν_1, ν_2, $\sigma_{\mu,1}$, $\sigma_{\mu,2}$). It can predict the difference $\mu_1 - \mu_2$ given a set of values for $\mu_1 + \mu_2$, ν_1, ν_2, $\sigma_{\mu,1}$, $\sigma_{\mu,2}$; only three of these five parameters are constrained by the measured input-output functions. Thus, the model is underconstrained for one value of contrast. However, experiments indicate that once neurons are adapted to a given value of contrast, parameters of experimentally measured nonlinearities increase approximately as a linear function of contrast [29, 25, 9, 16, 4]. We use this observation to fit the maximally informative model across contrasts. The resulting model has eight parameters altogether: the linear and offset terms with respect to contrast for each of the four noise terms (ν_1, ν_2, $\sigma_{\mu,1}$, $\sigma_{\mu,2}$). Because position of information maxima are affected by changes in any of these parameters, the maximally informative model can therefore be used to predict 27 independent measurements across contrasts (three values of $\mu_1 - \mu_2$, $\nu_{\text{eff},1}$, and $\nu_{\text{eff},2}$ for each contrast).

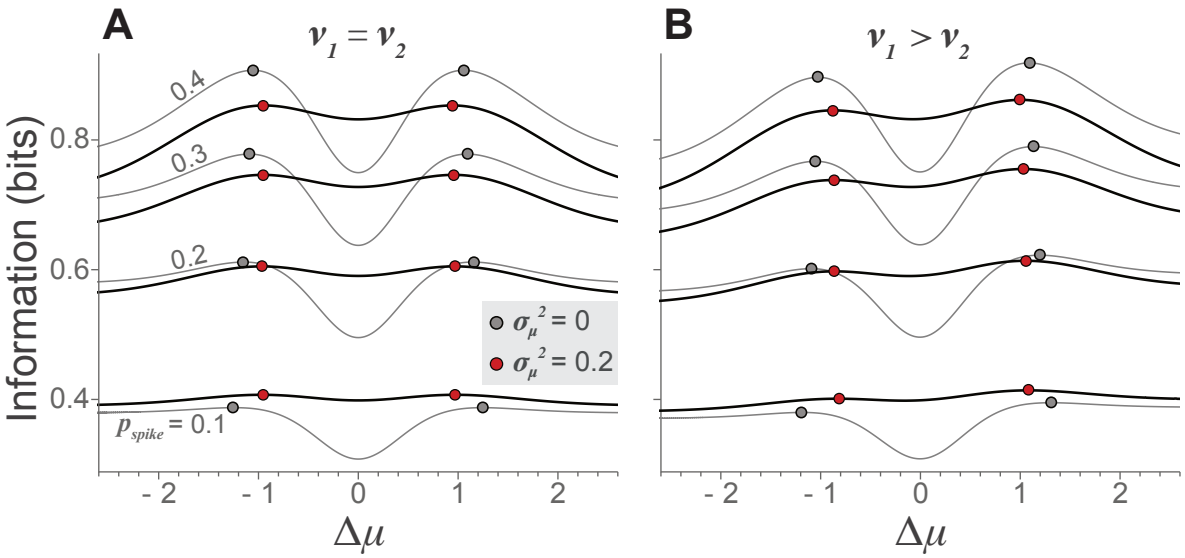

Figure B.1: **Long-term information surface.** The threshold modulation effectively smooths the information surface (thin lines, gray dots mark maxima) to give rise to the long-term information surface (thick lines, red dots mark maxima).

Appendix C

The effect of correlated noise on the optimal threshold separation

We also tested whether a model where the primary and secondary pathways simply sum with no nonlinear interaction could account for the data. In this case, the secondary pathway presents itself in the form of correlated noise variability between the adapting and sensitizing cells. Small, correlated variability has been observed in the retina [27, 1, 46], and its impact of information transmission has been studied [17, 54]. However, we now show that the correlated variability model cannot account for the observed threshold differences between neuronal types (assuming they are maximally informative or at least follow a local maximum of information).

First, we find that small positive correlations increase the optimal threshold separation between cell types, cf. Fig. C.1A. The negative correlations are largely not consistent with measurements [25], and in any case would not be able to reduce optimal threshold separation enough to match experimental measurements. In Fig. C.1B, we show that taking into account observed differences in the noise for the adapting and sensitizing cells further increases optimal threshold separation. This again shifts predictions in the direction opposite from the experimental measurements in Fig. 4.8. Thus, these results argue that the observed threshold differences

between RGCs need to be interpreted in the context of nonlinear threshold modulation.

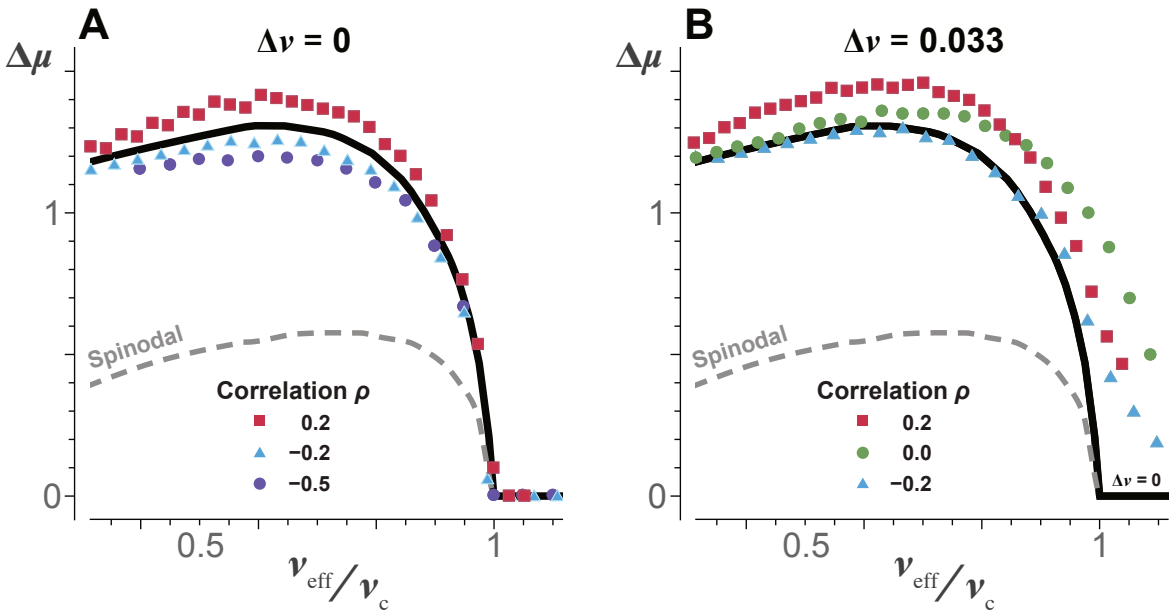

Figure C.1: **The effect of correlated noise on the optimal threshold separation between the neural types.** Equal (**A**) and unequal (**B**) noise levels for the two neurons in the pair. We only show points satisfying $\Delta\nu_{\text{eff}} \geq 0$ that would be consistent with the experimental observation of large effective noise in the adapting compared to sensitizing neurons. Positive correlations ($\rho > 0$) increase threshold separation. Although negative correlations reduce optimal threshold separation, the reduction is not sufficient to reach the area adjacent to the spinodal line and thus fail to explain the data.

Appendix D

Least-squared-fitting for parameters of the threshold modulation model from the retinal data

Base on the maximally informative modulation model, at a given $(\mu_1 + \mu_2)$ the solution to threshold difference between a pair of adapting and sensitizing cell, $\Delta\mu_{\text{model}}$, is nonlinearly dependent on the magnitude of each noise source (ν_i, $\sigma_{\mu,i}$). This allows us to separately estimate the magnitude of these noise components from the neural data.

The results of least-square fitting were also constrained to match the observed values for $\nu_{\text{eff},i}$. Seven pairs of adapting (index 1) and sensitizing cells (index 2) were probed by the nine different full range of contrasts ($\sigma = 12\%$ to 36% in 3% intervals [25]). The adaptive dynamics of noise level has been experimentally observed in many sensory systems [29, 25, 9, 16, 4]. Typically, the width of the transition region of the nonlinearity changes linearly with stimulus contrast (standard deviation). This adaptive process serves to optimize the information processing [9]. Here, we assume that both the primary (ν_i) and the secondary $\left(\sigma_{\mu,i}\right)$ noise

sources are approximately linearly dependent on contrast (σ),

$$\nu_i(\sigma,\vec{\alpha}) = \alpha_1^{(i)}\sigma + \alpha_2^{(i)}, \tag{D.1}$$

$$\sigma_{\mu,i}(\sigma,\vec{\alpha}) = \alpha_3^{(i)}\sigma + \alpha_4^{(i)}. \tag{D.2}$$

The effective noise also depends on contrast,

$$\nu_{\text{eff},i,\text{model}}(\sigma,\vec{\alpha}) = \sqrt{\nu_i^2(\sigma,\vec{\alpha}) + \sigma_{\mu,i}^2(\sigma,\vec{\alpha})}, \tag{D.3}$$

where $i = 1,2$ denotes adapting or sensitizing neuron, respectively. The parameters $\vec{\alpha} = \left\{\alpha_{1,2,3,4}^{(i)} \in R, \forall\, i = 1,2\right\}$ are to obtained by the least-squared-fitting for each cell pair while requiring them to also be consistent with $\nu_{\text{eff},i}$ measurements from the shape of the nonlinearity. This model has eight parameters. Although formally it can be fit to data points for each individual cell pair, we reduced the number of parameters in half by focusing on the dominant term between the linear and contrast-independent terms for each type of noise. Initial fitting of the model indicated very small values for $\alpha_2^{(1)}$, $\alpha_2^{(2)}$, $\alpha_4^{(1)}$, and $\alpha_3^{(2)}$. The final fitting reported here was obtained by setting these terms to zero, i.e., that noise in the primary pathway scales linearly with contrast for both types of cells; threshold modulation was set to be linearly increasing with contrast for adapting cells and to be contrast-independent for sensitizing cells.

The observed nonlinearities for a pair of adapting (index 1) and sensitizing cells (index 2) determine the threshold separations ($\Delta\mu = \mu_1 - \mu_2$) and the effective noise levels $\left(\nu_{\text{eff},1 \text{ or } 2}\right)$. For each cell pair, we aim to dissect two contributions to their $\nu_{\text{eff},1(\text{or } 2)}$: the one from the intrinsic noise level (ν) and that due to threshold modulation $\left(\sigma_\mu\right)$, via minimizing the squared-error between the retinal data and the model predictions across the nine contrasts ($\sigma = 12\%$ to 36% in 3% intervals). Given a contrast (σ) a data point of a cell pair, $\vec{O}(\sigma)$, consists of three

components,

$$\vec{O}(\sigma) = \left(\nu_{\text{eff},1}(\sigma), \nu_{\text{eff},2}(\sigma), \Delta\mu(\sigma)\right), \tag{D.4}$$

and so does our model $\vec{E}(\sigma, \vec{\alpha})$,

$$\vec{E}(\sigma, \vec{\alpha}) = \left(\nu_{\text{eff},1,\text{model}}(\sigma, \vec{\alpha}), \nu_{\text{eff},2,\text{model}}(\sigma, \vec{\alpha}), \Delta\mu_{\text{model}}(\sigma, \vec{\alpha})\right). \tag{D.5}$$

Here, $\Delta\mu_{\text{model}}(\sigma, \vec{\alpha})$ is the predicted threshold separation from our model, dependent on the intrinsic ν_i and modulatory noise $\sigma_{\mu,i}$ of each cell types,

$$\Delta\mu_{\text{model}}(\sigma, \vec{\alpha}) = \Delta\mu_{\text{model}}\left(\nu_1(\sigma, \vec{\alpha}), \nu_2(\sigma, \vec{\alpha}), \sigma_{\mu,1}(\sigma, \vec{\alpha}), \sigma_{\mu,2}(\sigma, \vec{\alpha})\right). \tag{D.6}$$

The predicted threshold differences ($\Delta\mu_{\text{model}}$) were firstly computed discretely in the grid space ($\nu_1, \nu_2, \sigma_{\mu,1}, \sigma_{\mu,2}$) and interpolated with Mathematica build-in function to construct the solutions between the grids. To avoid biasing the result by the component with largest error-bar, we standardize the $\left[\vec{O}(\sigma) - \vec{E}(\sigma, \vec{\alpha})\right]$ of each dimension with the inverse of its standard deviation. That is, the rescaling factors (weights) were

$$\vec{w} = 1/\left(\text{s.d.}\left(\nu_{\text{eff},1}\right), \text{s.d.}\left(\nu_{\text{eff},2}\right), \text{s.d.}\left(\Delta\mu\right)\right), \tag{D.7}$$

or more specifically,

$$w_i = \frac{1}{\text{s.d.}(O_i)} = \left[\frac{1}{N-1}\sum_{\sigma}\left(O_i(\sigma) - \langle O_i\rangle_{\sigma}\right)^2\right]^{-\frac{1}{2}}, \text{ for } i = 1 \text{ to } 3. \tag{D.8}$$

We defined the sum of weighted squared errors (or residuals) as

$$\chi^2(\vec{\alpha}) = \sum_{\sigma} \left| \vec{w} \odot \left[\vec{O}(\sigma) - \vec{E}(\sigma, \vec{\alpha}) \right] \right|^2, \tag{D.9}$$

where $\odot$ denotes component-wise multiplication. The parameter $\vec{\alpha}$ is the best-fit minimizing the weighted least-squared-error,

$$\vec{\alpha} = \arg\min_{\vec{\alpha}'} \chi^2\left(\vec{\alpha}'\right), \tag{D.10}$$

which predicts how the intrinsic (ν_i) and the modulation noise $\left(\sigma_{\mu,i}\right)$ depend on the stimulus contrast (σ). To quantify the goodness of fit, we use the variance (or reduced χ^2)

$$\chi^2_{\text{red}}(\vec{\alpha}) = \frac{\chi^2}{d.o.f.} = \frac{\chi^2}{N-n}, \tag{D.11}$$

where $d.o.f. =$ the number of degrees of freedom $= N - n$; N is the number of observations (nine contrasts in our case), and n is the number of fitted parameters. Note that by considering the threshold modulation, the predictions for the minimal threshold differences between the two cell types cannot go below the spinodal line. This makes it difficult to fit the data points adjacent to or below the spinodal region with our model. Therefore, the fitting results for three cell pairs did not adequately capture the trends (Fig. 4.8).

Finally, we also fit a single model across all cell pairs and contrasts. The resulting parameters (provided in the last row of Table D.1) were consistent with average values of parameters fitted to individual cell pairs (Fig. 4.7).

Table D.1: **Estimated noise components in the primary ν and modulatory σ_μ pathways for each cell pair.** The dependence of noise components upon the contrast are fitted by cell pair, across the nine contrasts ($\sigma = 12\%$ to 36% in 3% intervals). All the fitting parameters are in the unit of critical noise value, ν_c.

Cell pair #	Adapting		Sensitizing	
	$\nu_1(\sigma)$	$\sigma_{\mu,1}(\sigma)$	$\nu_2(\sigma)$	$\sigma_{\mu,2}(\sigma)$
A	0.819σ	0.281σ	0.784σ	0.0
B	0.671σ	0.546σ	0.749σ	0.049
C	0.713σ	0.448σ	0.801σ	0.025
D	0.413σ	0.618σ	0.545σ	0.051
E	0.670σ	0.598σ	0.758σ	0.010
F	0.604σ	0.528σ	0.622σ	0.033
G	0.482σ	0.751σ	0.594σ	0.013
Combined fit	0.597σ	0.563σ	0.685σ	0.033

Bibliography

[1] ALA-LAURILA, P., GRESCHNER, M., CHICHILNISKY, E. J., AND RIEKE, F. Cone photoreceptor contributions to noise and correlations in the retinal output. *Nat. Neurosci. 14*, 10 (2011), 1309–1316.

[2] ASHTON-JONES, B., AND COHEN, J. D. An integrative theory of locus coeruleus-norepinephrine function: adaptive gain and optimal performance. *Annu. Rev. Neurosci. 28* (2005), 403–50.

[3] ATICK, J. J., AND REDLICH, A. N. What does the retina know about natural scenes? *Neural Comput. 4* (1992), 196–210.

[4] BACCUS, S. A., AND MEISTER, M. Fast and slow contrast adaptation in retinal circuitry. *Neuron 36* (2002), 909–919.

[5] BALASUBRAMANIAN, V., AND STERLING, P. Receptive fields and functional architecture in the retina. *J. Physiol. 587*, 12 (2009), 2753–2767.

[6] BAR-YOSEF, O., AND NELKEN, I. The effects of background noise on the neural responses to natural sounds in cat primary auditory cortex. *Front. Comput. Neurosci. 1* (2007), 3.

[7] BIALEK, W. *Biophysics: Searching for principles*. Princeton University Press, Princeton and Oxford, 2012.

[8] BORGHUIS, B. G., RATLIFF, C. P., SMITH, R. G., STERLING, P., AND BALASUBRAMANIAN, V. Design of a neuronal array. *J. Neurosci. 28* (2008), 3178–3189.

[9] BRENNER, N., BIALEK, W., AND DE RUYTER VAN STEVENINCK, R. Adaptive rescaling maximizes information transmission. *Neuron 26*, 3 (2000), 695–702.

[10] BRENNER, N., STRONG, S. P., KOBERLE, R., BIALEK, W., AND DE RUYTER VAN STEVENINCK, R. R. Synergy in a neural code. *Neural Comput. 12* (2000), 1531–1552.

[11] BRINKMAN, B. A. W., WEBER, A. I., RIEKE, F., AND SHEA-BROWN, E. How do efficient coding strategies depend on origins of noise in neural circuits? *PLoS Comput. Biol. 12*, 10 (2016), e1005150.

[12] COVER, T. M., AND THOMAS, J. A. *Information theory*. John Wiley & Sons, INC., New York, 1991.

[13] COVER, T. M., AND THOMAS, J. A. *Elements of information theory*. John Wiley & Sons., 2012.

[14] DASARI, S., HILL, C., AND GULLEDGE, A. A unifying hypothesis for m1 muscarinic receptor signalling in pyramidal neurons. *J. Physiol. 595* (2017), 1711–1723.

[15] DOI, E., GAUTHIER, J. L., FIELD, G. D., SHLENS, J., SHER, A., GRESCHNER, M., MACHADO, T. A., JEPSON, L. H., MATHIESON, K., GUNNING, D. E., ET AL. Efficient coding of spatial information in the primate retina. *J. Neurosci. 32*, 46 (2012), 16256–16264.

[16] FAIRHALL, A. L., LEWEN, G. D., BIALEK, W., AND VAN STEVENINCK, R. R. D. R. Efficiency and ambiguity in an adaptive neural code. *Nature 412*, 6849 (2001), 787–792.

[17] FRANKE, F., FISCELLA, M., SEVELEV, M., ROSKA, B., HIERLEMANN, A., AND DA SILVEIRA, R. Structures of neural correlation and how they favor coding. *Neuron 89*, 2 (2016), 409–422.

[18] GARRIGAN, P., RATLIFF, C. P., KLEIN, J. M., STERLING, P., BRAINARD, D. H., AND BALASUBRAMANIAN, V. Design of a trichromatic cone array. *PLoS Comput. Biol. 6*, 2 (2010), e1000677.

[19] GJORGJIEVA, J., SOMPOLINSKY, H., AND MEISTER, M. Benefits of pathway splitting in sensory coding. *J. Neurosci. 34*, 36 (2014), 12127–12144.

[20] GOLLISCH, T., AND MEISTER, M. Eye smarter than scientistics believed: neural computations in circuits of the retina. *Neuron 65* (2010), 150–164.

[21] GORIS, R. L., MOVSHON, J. A., AND SIMONCELLI, E. P. Partitioning neuronal variability. *Nat. Neurosci. 17* (2014), 858–865.

[22] HAFT, M., AND VAN HEMMEN, J. L. Theory and implementation of infomax filters for the retina. *Network: Compt. Neural Syst. 9* (1998), 39–71.

[23] HARRIS, K. D., AND SHEPHERD, G. M. The neocortical circuit: themes and variations. *Nat. Neurosci. 18*, 2 (2015), 170–181.

[24] KASTNER, D., AND BACCUS, S. A. Insights from the retina into the diverse and general computations of adaptation, detection, and prediction. *Curr. Opin. Neurobiol. 25* (2014), 63–69.

[25] KASTNER, D. B., AND BACCUS, S. A. Coordinated dynamic encoding in the retina using opposing forms of plasticity. *Nat. Neurosci. 14*, 10 (2011), 1317–1322.

[26] KASTNER, D. B., AND BACCUS, S. A. Spatial segregation of adaptation and predictive sensitization in retinal ganglion cells. *Neuron 79*, 3 (2013), 541–554.

[27] KASTNER, D. B., BACCUS, S. A., AND SHARPEE, T. O. Critical and maximally informative encoding between neural populations in the retina. *PNAS 112*, 8 (2015), 2533–2538.

[28] KATO, H. K., CHU, M. W., ISAACSON, J. S., AND KOMIYAMA, T. Dynamic sensory representations in the olfactory bulb: modulation by wakefulness and experience. *Neuron 76* (2012), 962–975.

[29] LAUGHLIN, S. A simple coding procedure enhances a neuron's information capacity. *Z. für Naturforschung 36* (1981), 1432–1438.

[30] LAUGHLIN, S. B. Energy as a constraint on the coding and processing of sensory information. *Curr. Opin. Neurobiol. 11*, 4 (2001), 475–480.

[31] LAUGHLIN, S. B., DE RUYET VAN STEVENINCK, R. R., AND ANDERSON, J. C. The metabolic cost of neural computation. *Nat. Neurosci. 41* (1998), 36–41.

[32] LIGUZ-LECZNAR, M., URBAN-CIECKO, J., AND KOSSUT, M. Somatostatin and somatostatin-containing neurons in shaping neuronal activity and plasticity. *Front. Neural Circuits 10* (2016), 48.

[33] LIU, Y. S., STEVENS, C. F., AND SHARPEE, T. O. Predictable irregularities in retinal receptive fields. *PNAS 106* (2009), 16499–16504.

[34] LUCK, S. J., CHELAZZI, L., HILLYARD, S. A., AND DESIMONE, R. Neural mechanisms of spatial selective attention in areas v1, v2, and v4 of macaque visual cortex. *J. Neurophysiol. 77* (1997), 24–42.

[35] MANU, M., AND BACCUS, S. A. Disinhibitory gating of retinal output by transmission from an amacrine cell. *PNAS 108*, 45 (2011), 18447–18452.

[36] MCDONNELL, M. D., STOCKS, N. G., PEARCE, C. E., AND ABBOTT, D. Optimal information transmission in nonlinear arrays through suprathreshold stochastic resonance. *Phys. Lett. A 352*, 3 (2006), 183–189.

[37] MORRONE, M. C., BURR, D. C., AND MAFFEI, L. Functional implications of cross-orientation inhibition of cortical visual cells. 1. neurophysiological evidence. *Proc. Royal Soc. B 216* (1982), 335–354.

[38] NIKITIN, A., STOCKS, N.G.AND MORSE, R. P., AND MCDONNEL, M. D. Neural population coding is optimized by discrete tuning curves. *Phys. Rev. Lett. 103* (2009), 138101.

[39] NISHIMOTO, S., ISHIDA, T., AND OHZAWA, I. Receptive field properties of neurons in the early visual cortex revealed by local spectral reverse correlation. *J. Neurosci. 26* (2006), 3269–3280.

[40] OLSHAUSEN, B. A., AND FIELD, D. J. Sparse coding of sensory inputs. *Curr. Opin. Neurobiol. 14*, 4 (2004), 481–487.

[41] OLSHAUSEN, B. A., AND FIELD, D. J. How close are we to understanding V1? *Neural Comp. 17* (2005), 1665–1699.

[42] PITKOW, X., AND MEISTER, M. Decorrelation and efficient coding by retinal ganglion cells. *Nat. Neurosci. 15* (2012), 628–635.

[43] RATLIFF, C. P., BORGHUIS, B. G., KAO, Y.-H., STERLING, P., AND BALASUBRAMANIAN, V. Retina is structured to process an excess of darkness in natural scenes. *PNAS 107*, 40 (2010), 17368–17373.

[44] RIEKE, F., WARLAND, D., DE RUYTER VAN STEVENINCK, R., AND BIALEK, W. *Spikes: Exploring the Neural Code*. MIT Press, Cambridge, MA, USA, 1999.

[45] ROELFSEMA, P. R. Cortical algorithms for perceptual grouping. *Annu. Rev. Neurosci. 29* (2006), 203–227.

[46] SCHNEIDMAN, E., BERRY II, M. J., SEGEV, R., AND BIALEK, W. Weak pairwise correlations imply strongly correlated network states in a neural population. *Nature 440* (2006), 1007–1012.

[47] SIMMONS, K. D., PRENTICE, J. S., TKAČIK, G., HOMANN, J., YEE, H. K., PALMER, S. E., NELSON, P. C., AND BALASUBRAMANIAN, V. Transformation of stimulus correlations by the retina. *PLoS Comput. Biol. 9*, 12 (2013), e1003344.

[48] URBAN-CIECKO, J., AND BARTH, A. L. Somatostatin-expressing neurons in cortical networks. *Nat. Rev. Neurosci. 17*, 7 (2016), 401.

[49] VINJE, W. E., AND GALLANT, J. L. Sparse coding and decorrelation in primary visual cortex during natural vision. *Science 287* (2000), 1273–1276.

[50] VINJE, W. E., AND GALLANT, J. L. Natural stimulation of the nonclassical receptive field increases information transmission efficiency in V1. *J. Neurosci. 22* (2002), 2904–2915.

[51] WANG, Z., WEI, X.-X., STOCKER, A. A., AND LEE, D. D. Efficient neural codes under metabolic constraints. In *Adv. Neural Inf. Process. Syst.* (2016), pp. 4619–4627.

[52] YI, F., BALL, J., STOLL, K., SATPUTE, V., MITCHELL, S., PAULI, J., HOLLOWAY, B., JOHNSTON, A., NATHANSON, N., DEISSEROTH, K., GERBER, D., TONEGAWA, S., AND LAWRENCE, J. Direct excitation of parvalbumin-positive interneurons by m1 muscarinic acetylcholine receptors: roles in cellular excitability, inhibitory transmission and cognition. *J. Physiol. 592* (2016), 16.

[53] ZHAOPING, L. Theoretical understanding of the early visual processes by data compression and data selection. *Network 17* (2006), 301–334.

[54] ZYLBERBERG, J., CAFARO, J., TURNER, M. H., SHEA-BROWN, E., AND RIEKE, F. Direction-selective circuits shape noise to ensure a precise population code. *Neuron 89*, 2 (2016), 369–383.